SAPIENZA
Università di Roma
Facoltà di Scienze Matematiche Fisiche e Naturali

DOTTORATO DI RICERCA
IN GENETICA E BIOLOGIA MOLECOLARE

XXXIII Ciclo
(A.A. 2019/2020)

Structural and epigenetic dysfunctions of telomeric chromatin in cancer cells

Dottorando
Angela Dello Stritto

Docente guida
Prof. Stefano Cacchione

Tutore
Dr Annamaria Biroccio

Coordinatore
Prof. Fulvio Cruciani

INDEX

GLOSSARY

3'-overhang: single-stranded protruding of the telomeric G-rich strand at the 3'-end of the chromosome.

ALT: Alternative Lengthening of Telomeres, a telomerase independent telomere maintenance mechanism based on Homologous Recombination.

ATM (Ataxia Telangiectasia Mutated): kinase involved in DNA damage signaling at DNA double-strand breaks.

ATR (Ataxia Telangiectasia and Rad3-related): kinase involved in DNA damage signaling at DNA single-strand breaks. It is activated after RPA recognition of unprotected ssDNA.

ATRX/DAXX: Alpha thalassemia/mental retardation syndrome X-linked chromatin remodeler (ATRX), DAXX (death domain-associated protein), are histone chaperone involved in H3.3 deposition.

CRC: colon-rectal cancer.

DDR (DNA Damage Response): a series of pathways activated by the presence of DNA damage.

DNMT3A/B: DNA (cytosine-5-)-methyltransferase 3, are members of the family of DNMTs, which catalyze the addition of methyl groups to cytosine residues of CpG dinucleotides.

EMSA: electrophoretic mobility shift assay.

G-quadruplex: a four-stranded DNA structure derived by the establishment of four planar Hoogsteen bonds between four

guanines (G-quartet) followed by the stacking of three or four G-quartets.

H3.3: Variant of the Histone H3, deposed in a cell-cycle independent manner, at highly transcribed genes and at heterochromatic regions.

ITS: Interspersed Telomeric Sequences.

MNase: Micrococcal endo-exo nuclease derived from Staphylococcus aureus. This enzyme is able to produce double-strand breaks within nucleosome linker regions. The efficiency depends on the degree of chromatin compaction.

NCP: Nucleosome Core Particle

R-loops: three-stranded nucleic acid structure, composed of a DNA:RNA hybrid and the associated non-template single-stranded DNA

Shelterin: protein complex involved in maintenance and protection of mammalian telomeres.

t-loop (telomere loop): lariat-like structure derived from the 3'-overhang invasion of an upstream double-stranded region at telomeres

SIRT6: nicotinamide adenine dinucleotide^{+} (NAD^{+}) dependent sirtuin, is involved in stress response and in telomeres homeostasis maintenance.

SUV39H1/2: Suppressor of Variegation 3-9 Homolog (1-2), are Histone-lysine N-methyltransferases.

Telomerase: ribonucleoprotein complex that synthesizes new telomeric repeats at the chromosome ends. Its RNA component (TERC) has a sequence that shows complementarity with the G-rich telomeric sequence and can pair with the 3'-overhang, while its protein component (TERT) has reverse transcription activity.

Telomeres: nucleoprotein complexes localized at the end of eukaryotic linear chromosome. They allow the cell to distinguish chromosome ends from DNA double strand breaks.

TERRA: Long noncoding RNA transcribed from telomeres, which associates with several telomeric components, such as TRF2 and telomerase.

TMMs: Telomere Maintenance Mechanisms.

TIN2 (TRF2- and TRF1-Interacting Nuclear protein 2): mammalian telomeric protein that bridges TRF1 and TRF2 to the heterodimer TPP1/POT1.

TPE: telomere position effect.

TPE OLD: telomere position effect over long distance.

TPP1 (TINT1, PTOP and PIP1): mammalian telomeric protein that form a subcomplex with POT1, recruiting it to telomeres and increasing its ssDNA binding affinity.

TRF1 and TRF2 (Telomeric Repeat binding factor 1 and 2): mammalian telomeric proteins that bind dsDNA and allow assembly of the Shelterin complex. TRF2 is involved in repression of ATM-mediated DDR.

SUMMARY

Telomeres are the nucleoprotein structures that protect chromosome termini in eukaryotes. Functional telomeres need the establishment of a protective chromatin structure based on the interplay between the specific complex named shelterin and a tight nucleosomal organization. In somatic cells, progressive telomere reduction brings to the destabilization of the telomere capping structure and to the activation of a DNA damage response (DDR) signaling. Then, cells enter into replicative senescence, which constitute a protective barrier against unlimited proliferation. A crucial step in cancer development is the acquirement of a telomere maintenance mechanism that gives the neoplastic cell unlimited replicative potential, one of the main hallmarks of cancer. Despite the crucial role that telomeres play in cancer development, little is known about the epigenetic alterations of telomeric chromatin that affect telomere protection and are associated with tumorigenesis.

Here, we explore two different aspects of the role of telomeric chromatin and its dysfunctions in cancer development. The first aspect concerns the interaction between SIRT6 deacetylase and the telomeric protein TRF2 in heterochromatin stability and cancer. It has been previously reported that TRF2 is a substrate of SIRT6, and that an inverse correlation between SIRT6 and TRF2 protein expression levels was present in a cohort of CRC patients (Rizzo et al., 2017). To investigate the dynamic and the effects of this interaction we performed several *in vitro* binding assays that showed that SIRT6 has the capability of stabilize the interaction of TRF2 with the telomeric nucleosome *in vitro*. Additionally, chromatin extractions after silencing SIRT6 in HCT cancer cell indicate that SIRT6 stabilizes TRF2 binding to chromatin also in vivo. Then, we performed chromatin immunoprecipitation of TRF2 coupled with sequencing (ChIP-seq) in HCT-116 cells upon SIRT6 silencing. We found that TRF2 delocalize both from telomeres and from pericentromeres. Furthermore, we also found an increased TRF2 binding on several gene promoters involved in cancer development

upon SIRT6 depletion. Collectively these data unveil new interesting elements about the interplay of SIRT6 and TRF2 with heterochromatin in colon cancer cells, which could be relevant for a deeper understanding of the mechanisms of tumor onset and potentially brings to the development of new anti-cancer therapies.
The second aspect regards the role played by the histone variant H3.3 at telomeres. Among the histone variants, H3.3 is the most common non-centromeric variant of histone H3. Besides being a mark of transcriptionally active regions, it is also enriched at pericentromeres and telomeres.
Some dominant mutations in the H3F3A/B genes have been described in several paediatric cancers. Interestingly, a positive correlation with mutations in chaperones responsible for H3.3 deposition at telomeres and pericentromeres, and an association with ALT phenotype was also reported. Thus, unravelling H3.3 function(s) at telomeres could be pivotal for both basic and applied research.
A detailed analysis of telomeric chromatin organization is still lacking, mainly because of the complex nature of human telomeres, characterized by high length heterogeneity and low sequence complexity. To overcome the difficulties generated by the uniformly repeated telomeric sequence, we developed a strategy to map nucleosome positions using subtelomeric sequences as starting point. We generated transgenic cell lines expressing a H3.3Q85C mutated gene. This particular mutation makes chromatin sensitive to treatment with phenantroline/copper/H_2O_2, which cuts nucleosomal DNA twenty-five base pairs from the dyad axis. To characterize the fragments of different length emerging from MNase or chemical cleavage, we took advantage of Oxford Nanopores, a sequencing technique that can handle very long fragments and does not require any amplification step. We performed pilot sequencing runs of MNase digested DNA to test the feasibility of nanopores to map telomeric nucleosome positions and spacing. The analysis of the read lengths showed clearly that nucleosome spacing at telomeres is shorter than in the rest of chromatin, but the number of

reads obtained is too small to allow nucleosome mapping of single telomeres. For this reason, we developed a protocol to enrich telomeric DNA, by using biotinylated telomeric probes and streptavidin magnetic beads to capture telomeric sequences. With the application of these tools, we aim – in the near future - to obtain a detailed map of telomeric (and genome wide) H3.3 containing nucleosomes and to develop a reliable method to study the H3.3 mutations found in ALT and paediatric cancers.

INTRODUCTION

Switching from circular to linear chromosome, eukaryotes had to solve two main problems. First, the new chromosome termini had to prevent processing from the DNA repair system as broken DNA ends. Second, avoiding the loss of genetic material consequent to the incomplete replication of the very ends of chromosomes. To overcome these obstacles, cells evolved the nucleoprotein structures called telomeres.

TELOMERES

In most eukaryotes telomeric DNA consists of arrays of short tandem repeats enriched in guanine (Blackburn, 1991). Mammalian telomeres comprise several kilobase pairs (kb) of TTAGGG repeats, ending in a single-stranded G-rich 3'-overhang up to 500 nt long (Makarov et al., 1997). This peculiar DNA sequence structure co-evolved with specific protein and nucleoprotein complexes to ensure both protection from DNA damage signaling and the complete replication of chromosomal DNA.
Protection is assured by the Shelterin complex, that in humans consists of six proteins: TRF1, TRF2, Rap1, TIN2, POT1, TPP1 (de Lange, 2005; Liu et al., 2004). DNA damage response (DDR) is inhibited by Shelterin and by the formation of t-loops, a configuration of telomeric DNA in which the G-rich overhang folds back and invades the double-stranded upstream telomeric DNA, forming a lariat structure (Palm and de Lange, 2008).

- **The Shelterin complex**

In details, TRF1 and TRF2 tie up to double-stranded telomeric DNA (Liu et al., 2004), POT1 anchors to the single-stranded protrusion (Baumann and Cech, 2001; Lei et al., 2004), TIN2 connects TRF1, TRF2 and TPP1, which in turn binds POT1. Lastly, Rap1 interacts only with TRF2 (Xin et al., 2008).

In human and mouse cells, TRF1, TRF2, TIN2, and Rap1 are about 10 times richer than TPP1 and POT1. The abundance of the core of Shelterin is sufficient to bind all double stranded telomeric repeats, and there is a tenfold excess of TPP1/POT1 over its binding sites, suggesting that most of the telomeric DNA is associated with Shelterin proteins (Takai et al., 2010).

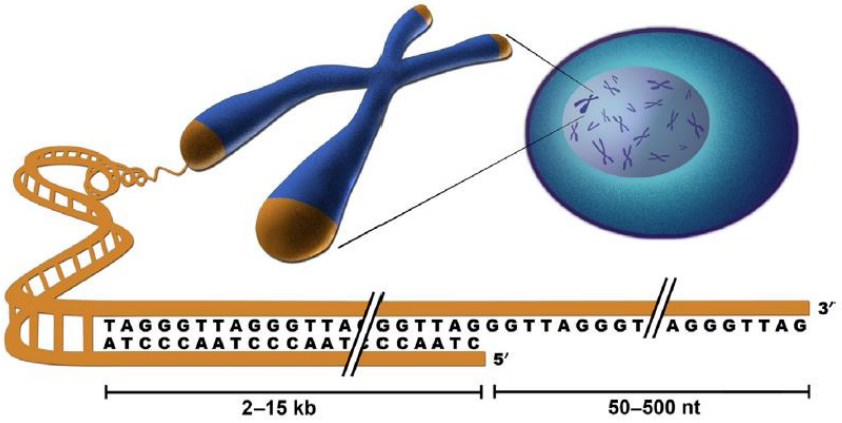

Fig. 1. Schematic representation of telomeres. In vertebrates, telomeric DNA is constituted by several kilobase pairs of TTAGGG repeats, and a 3' -single stranded overhang of 50-500 bp long overhang (Micheli, E. et al., 2016).

Even though these protein components are considered as subunits of a greater complex, they exert their functions pretty autonomously from each other in maintaining telomeric homeostasis. The TRF2 subunit is involved in inhibition of the ATM-dependent damage signaling pathway and of the c-NHEJ (Bae and Baumann, 2007; Celli and de Lange, 2005; Karlseder et al., 1999). POT1 acts as a repressor of the ATR kinase signaling pathway and of the HR in a concerted action with Rap1 (Gong and de Lange, 2010). POT1 and TRF2 act independently to restrain two different 5' resection pathways at telomere termini. (Denchi and de Lange, 2007).
TRF1 is involved in promoting the semi-conservative replication of telomeres (Sfeir et al., 2009). TPP1 is instead a positive regulator of telomere maintenance and has a role in recruiting telomerase (Abreu

et al., 2010), which is, at the same time, negatively regulated by Shelterin complex for the maintenance of proper telomere length (van Steensel and de Lange, 1997).

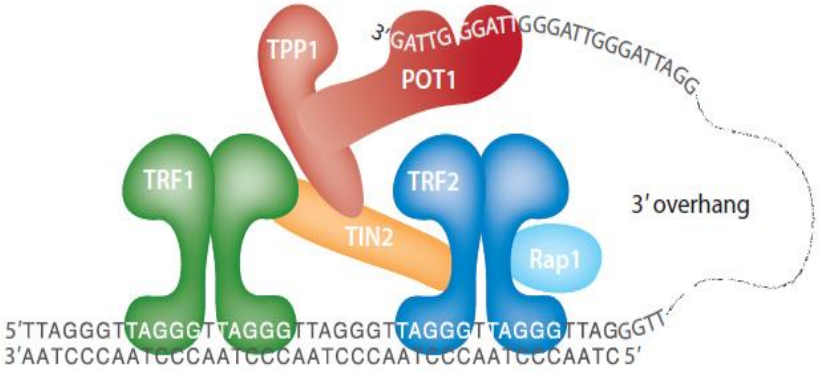

Fig. 2. Structure of the Shelterin complex. TRF1 and TRF2 are directly associated with the dsTTAGGG, POT1 is bounded to the 3'overhang. TPP1 and TIN2 mediate the alliance between POT1 and TRF1/TRF2 dimers. Lastly, Rap1 interacts only with TRF2 (de Lange, 2018).

Shelterin regulates these and other processes by employing several co-factors that are transiently recruited at telomeres.
For the G-overhang processing, it is required the concerted action of the Shelterin complex, Apollo, Exo1 (both nucleases) and of the CTC1-STN1-TEN1 (CST) complex (Wu et al., 2012).
To ensure the proper replication of telomeres, that are hard-to-replicate regions of chromosomes, Shelterin interacts with distinct helicases, such as BLM, that can resolve G-quadruplex DNA structure (Liu et al., 2010) or RTEL1, which assists the replication of the leading strand (Uringa et al., 2012; Vannier et al., 2012). All of these DNA processing activities must be limited and tightly controlled by Shelterin.

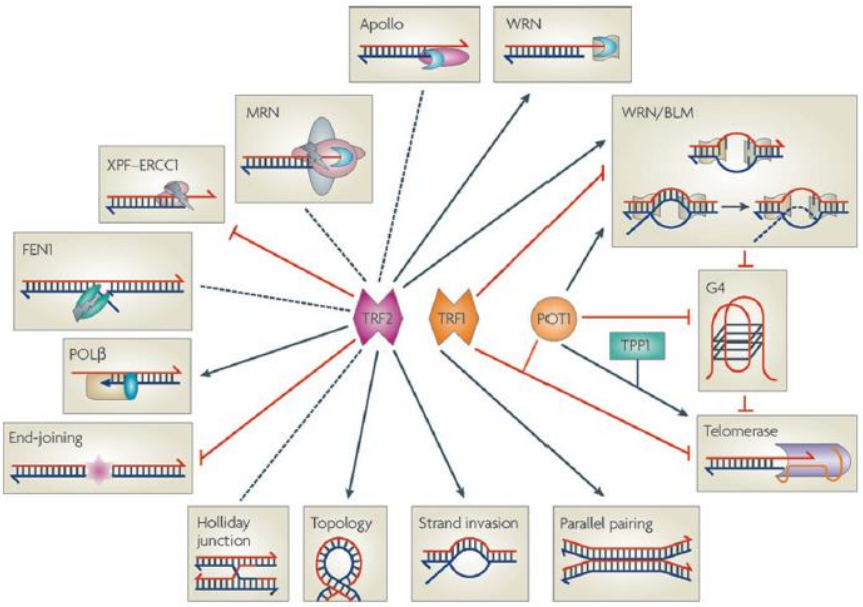

Fig. 3. The Shelterin subunits exert several enzymatic activities and regulate many facets of telomeric homeostasis, by acting as activators of the processes (black arrow), or as repressors (red line) (Gilson and Geli, 2007).

TELOMERIC DNA FEATURES: TRANSCRIPTION AND SECONDARY STRUCTURES

- **Transcription of telomeric DNA: TERRA**

Although telomeres have been for long time considered heterochromatic, they are transcribed and produce long non-coding RNAs called TERRA (telomeric repeat containing RNA).
TERRA is a lncRNA composed by 5'-UUAGGG-3' repeats (Azzalin et al., 2007; Schoeftner and Blasco, 2008), ranging in length between 100 bp and 9 kb in mammals (Azzalin et al., 2007; Porro et al., 2010). Its transcriptional rate is cell-cycle dependent, with the higher peak during the early G1 and the lower peak during the late S phase, concurrently with telomeres replication. Biogenesis and functions of TERRA are subject of heated debate in scientific community. It is known that TERRA depletion trough antisense oligonucleotides (ASO) leading to increased DNA damage at telomeres, suggesting an involvement in genomic structural integrity. Moreover, live-cell imaging in a human cancer cell line showed TERRA molecules diffuse in the nucleus. These evidences suggest an action "in trans" of this long non coding RNA, supported also by the presence of DNA damage not only limited at telomeres, but extended to the genome upon its depletion (Avogaro et al., 2018).
However, even if some RNA FISH show the association of the lncRNA at all telomeres, is still unclear if TERRA is actually transcribed from all subtelomeres (Azzalin et al., 2007; Feretzaki et al., 2019; Porro et al., 2014) or from only few ones (Lopez de Silanes et al., 2014; Montero et al., 2016), even though TERRA promoter sequences have been described (Nergadze et al., 2009). Notably, as other long non coding RNAs, it has been demonstrated the co-existence of polyA- and polyA+ versions of it, with a different sub-nuclear localization, suggesting that TERRA-poly-A(+) and poly-A(-) might exert distinct functions (Porro et al., 2010).

In addition, TERRA can associate with telomerase RNA, followed by an event of nucleation during the early S-phase. Then, this TERRA-telomerase complex is tethered on the shortened telomere from which TERRA molecules were transcribed (Cusanelli et al., 2013).
The well documented presence of TERRA at telomeres, and also its upregulation in ALT cancer cells, suggests its involvement in telomeres homeostasis, although the role of TERRA in the establishment of telomeric heterochromatin is still controversial (Barral and Dejardin, 2020). It has been shown that TERRA interacts with HP1α, TRF1, TRF2 and with the origin recognition complex (ORC) (Deng et al., 2009), recruits the Polycomb repressive complex 2 (PRC2) to telomeres in order to methylate H3K27 and SUV39H1 which are in turn necessary for telomeric heterochromatin formation (Porro et al., 2014). It is known that telomeric transcriptional activity can bring to the formation of local TERRA-telomeres DNA hybrids, which are fated to provoke replication stress through the formation of R-loops. Moreover, TERRA can form G-quadruplex structures, similarly to telomeric G-rich DNA (Martadinata et al., 2011; Xu et al., 2008). At first glance these structures could be defined as merely harmful, actually have very important functions for the proper execution of several biological processes.

- **G-Quadruplex**

Due to its G composition, the 3'-overhang of telomeres can fold in non-canonical secondary structures named G-quadruplex (G4), formed by assembling the G-tracts into three stacked G-tetrads, planar arrangements of Gs in Hoogsteen hydrogen bonding interactions. The G4 is a helical structure with a right-handed orientation, where every G in the tetrad, for what regards the canonical structure, is rotated 90° with respect to the near ones. G4s are often composed by four tracts of three Gs (G3), but sequences

with longer (G4-7), shorter (G2) G-tracts are also permissive for structure formation (Burge et al., 2006).

G quadruplexes are found throughout the genome and in mRNA, at gene promoters, telomeres, and telomeric or virus RNA (Harkness and Mittermaier, 2017). Over 375,000 sequences have been identified within the human genome that have the potential to form G-quadruplexes (Huppert and Balasubramanian, 2005).

In humans, G4s are involved in regulation of several processes, such as replication, gene expression, inhibition of recombination, splicing, telomere protection and extension (Rhodes and Lipps, 2015). The presence of G-quadruplexes along the DNA can stall replication forks, causing replication stress and eventually DNA damage in absence of dedicated helicases, as well as FANCJ, BLM and WRN, which are necessary for G4 resolving (Rhodes and Lipps, 2015; Zhang et al., 2019) . Beyond recruitment of helicases, G4s can call up also heterogenous ribonucleoprotein U (hnRNP U), which has been proven to be a G4 binding protein. hnRNP U prevents replication protein A (RPA) accumulation at telomeres, and the recognition of telomeric ends by hnRNP suggests that a G-quadruplex promoting protein regulates its accessibility (Izumi and Funa, 2019).

For a long time it was thought that at telomeres the intramolecular folded G4s may offer end protection against nucleases or regulate telomerase activity (Zahler et al., 1991), raising great interest in G4 stabilizers and in their inhibitory action towards telomerase.

However, G4 ligands, still remains an effective potential anticancer therapy. Stabilization of G4 leads to telomere dysfunctions and deleterious effect on cellular growth, which render G4 ligands, such RHPS4 (Berardinelli et al., 2018; Berardinelli et al., 2015; Salvati et al., 2007) and Pyridostatin (Zimmer et al., 2016), good candidates for chemotherapeutic purposes.

- **R-Loops**

R-loops are three-stranded structures formed by a DNA:RNA hybrid and a displaced DNA strand (Tan and Lan, 2020). This type of structures arises during the transcriptional process, when the 5' end of the RNA being transcribed reinvades the double helix temporarily opened due to the passage of the RNA polymerase. R-loops are very strong structures and, once formed, it is necessary the intervention of helicases for their resolution (Niehrs and Luke, 2020).
R-loops formation is favored by the presence of CG-skew sequences, so they can be found enriched at telomeres (Moyzis et al., 1988; Tan et al., 2020), where the TTAGGG double strand undergoes to invasion from long noncoding TERRA, which hybridizes with the C-rich strand (Rippe and Luke, 2015). In yeast, R-loops are stabilized by critical telomere shortening, which drives recombination by promoting recruitment of RAD51 (Graf et al., 2017). Moreover, it has been shown that the presence of ATRX at telomeres is crucial for R-loops resolution (Nguyen et al., 2017) as well as NONO and SFPQ, two TERRA binding proteins which have a role in suppressing RNA:DNA hybrids at telomeres (Petti et al., 2019).
As G-quadruplexes, these secondary structures seem detrimental for cell physiology. The current view is that R-loops could threaten genome integrity if present at abnormally high levels, while they are likely to play regulative roles when tightly regulated (Niehrs and Luke, 2020).

MECHANISMS OF MAINTENANCE OF TELOMERE LENGTH

Protection of chromosome ends includes preventing the loss of genomic material during the replication process, caused by the inability of DNA polymerases to fully replicate the ends of the linear chromosomes (Olovnikov, 1973). Indeed, telomeres shorten by ~50 bps with each cell division because of the "end replication problem".

In absence of a mechanism of compensation and re-elongation of TTAGGG repeats, cells go towards a senescence-phase (Herbig et al., 2004; von Zglinicki et al., 2005).
In the vast majority of eukaryotes, the process of end-erosion is thwarted by the telomerase, which adds short repeats to the 3' extremities of telomeres (Blackburn, 1992). In humans, telomerase is active only in stem and germinal cells. In somatic cells, telomerase activity is downregulated through the silencing of TERT (the reverse transcriptase subunit of the telomerase) (Maciejowski and de Lange, 2017). Consequently, somatic cells go towards a programmed telomere shortening with each cell cycle (Cristofari and Lingner, 2006). When the chromosome ends reach a critical length, the loading of the Shelterin become insufficient to maintain of the closed conformation. Unprotected telomeres trigger DDR and the blockage of cell replication; cell fate is replicative senescence or apoptosis (Mortality stage 1, M1) (Maciejowski and de Lange, 2017; Shay, 2016). Due to the heterogeneity in telomere length, few telomeres critically short are sufficient to cause replicative arrest (Gilson and Londono-Vallejo, 2007).
If the checkpoints necessary for cell cycle arrest, such as p53 and RB pathways are inactivated, cells overcome the proliferative block and continue to divide, bringing telomeres to be completely deprotected. This condition, called Telomere crisis or Mortality stage M2, is characterized by the total absence of the Shelterin, which causes the activation of the DNA repair mechanisms and generates end-to end fusions, dicentric chromosomes and other forms of genomic instability (Maciejowski and de Lange, 2017; Shay, 2016). These major chromosomal rearrangements generally lead to massive cell death.
Rarely, mutations might lead to the activation of a telomere-maintenance mechanism, which gives to cells the capability to circumvent the crisis with re-stretched telomeres, re-establishing stability on a rearranged genome, and an unlimited proliferative potential, all typical features of cancer cells.

In the vast majority of human tumors, immortalization of cancer cells arises by the reactivation or upregulation of telomerase; indeed, telomerase activity is detected in 85-90% of all malignant tumors (Kim et al., 1994). In the remaining 10-15%, telomere attrition is reversed by a different mechanism based on recombination named Alternative Lengthening of Telomeres (ALT) (Pickett and Reddel, 2015).

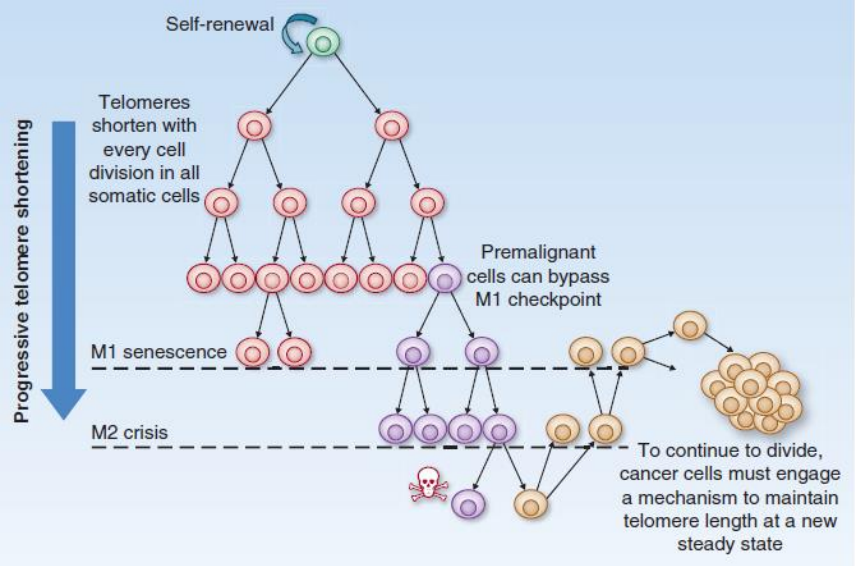

Fig. 4. Telomere erosion occurs with each cell cycle, until they reach a critical length which triggers senescence process, or mortality stage (M1). Some premalignant cells may overcome this step by obtaining enough oncogenic mutations, entering in an extended lifespan period and then in M2 crisis, where the most of cells die. Rare cells acquire a mechanism to maintain telomere length by telomerase reactivation or though activation of the ALT pathway, a necessary step toward neoplastic onset (Shay, 2016).

- **Telomerase**

Telomerase is a ribonucleoprotein (RNP) complex composed by two main different subunits: a specialized telomerase reverse transcriptase (TERT) and an RNA template known as telomerase RNA component (TERC) containing the template for telomere elongation (Blackburn, 1992; Feng et al., 1995; Wu et al., 2015). In

humans, telomerase is recruited by the Shelterin complex. Through an interaction with TPP1, telomerase makes both transient and stable association with each telomere several times during S-phase, but only few times forms strong association (Schmidt et al., 2016). Some studies of single molecule tracking showed that the RNA component of telomerase (hTR) is restrained in Cajal bodies, which are involved in telomerase biogenesis and recruitment to chromosome ends (Chartrand and Sfeir, 2020).
The association between the telomeric G-overhang and hTR favors the stable interaction necessary for the proper telomerase association at chromosome ends. This recruitment is mediated by TPP1.
telomerase loading to telomeres then yields the partial pairing of the RNA template with the DNA overhang, and the positioning of the telomeric DNA 3'-end at the active site of TERT. When the replication of one repeat is complete, the RNA–DNA hybrid briefly disconnect to permit the pairing of the DNA overhang with the distal region of the RNA-templating region, so that the replication of another telomeric repeat can be initiated (Mason et al., 2011)
Recently, it has been shown that telomerase has also noncanonical function, namely promoting cancer cells proliferation, and assembling a telomere protective complex comprising Hsp70-1 and Apollo (Perera et al., 2019). Telomerase activity is detected in 85-90% of all malignant tumors: somatic mutations in the proximal promoter of hTERT are now considered the most common (31%) non-coding mutation in cancer. However, hTERT amplifications (3%), hTERT structural variants (3%) and hTERT promoter methylation (53%) have been identified as well. (Kim et al., 1994; Shay and Bacchetti, 1997).

- **ALT mechanism**

Homologous Recombination is involved in the ALT mechanism, which provides a way to maintain telomeres in the absence of telomerase (Bryan et al., 1995).
Even if the ALT mechanism has not been completely described, it is thought that the chromosome 3'-end invades the homologous

chromosomal telomere, miming a primer and allowing the replication of the donor DNA and re-elongation of the telomeric repeats. HR-related proteins, as well as MRN complex, Rad51, Rad52, FANC are thus necessary for telomere conservative replication (Cesare and Reddel, 2010). A consistent number of 3' telomeric ends likely derives by an increased proneness of ALT telomeres to replication stress, leading to DSB and break-induced telomere synthesis (Cesare and Reddel, 2010; Doksani and de Lange, 2016).

The establishment of ALT is probably triggered by increased replication stress and DSBs but needs a favorable genetic background. The most frequent mutations associated with ALT are in the genes ATRX and DAXX (Heaphy et al., 2011; Lovejoy et al., 2012). The complex ATRX/DAXX mediates the incorporation at telomeres and at other repeated regions of the histone variant H3.3 (see section: Histone variant H3.3, page 28). However, mutations in ATRX are not sufficient to induce ALT. The epigenetic status of ALT telomeres is still matter of discussion (De Vitis et al., 2018).

Previous reports showed decondensed chromatin and a decrease of the heterochromatic mark H3K9me3 in ALT telomeres (Episkopou et al., 2014). Conversely, other reports showed an enrichment in heterochromatic marks at telomeres in ALT cell lines (Cubiles et al., 2018)(Gauchier et al., 2019).

ALT positive cells show a phenotype with a certain degree of heterogeneity, but with some particular features encountered very frequently, such as the loss of ATRX/DAXX functions (Clynes et al., 2015), high number of ALT-associated PML bodies (APBs) (Yeager et al., 1999), high number of extra-chromosomal telomeric repeat DNA (ECTR) (Cesare and Griffith, 2004), T-circles and C-circles (Oganesian and Karlseder, 2013), unpaired telomeric sister chromatid exchange (T-SCE) (Londono-Vallejo et al., 2004) and the increasing level of TERRA transcription (Episkopou et al., 2014).

ALT is spread principally in tumors of the nervous system and in sarcomas (Dilley and Greenberg, 2015), and between cancers that derive from mesenchymal tissues; 47% of osteosarcomas, 35% of

soft-tissue sarcomas (STS) and 80% of pleomorphic liposarcoma have been shown to utilize the ALT mechanism (Henson et al., 2005).

TELOMERIC CHROMATIN

Mammalian telomeres have a peculiar chromatin structure, which is characterized by tightly packed nucleosomes (Makarov et al., 1993; Tommerup et al., 1994) , by the presence of heterochromatic marks, such as H3K9me3 (Garcia-Cao et al., 2004) and H4K20me3 (Benetti et al., 2007b; Marion et al., 2011) and by the enrichment of the H3.3 variant (Goldberg et al., 2010; Udugama et al., 2015).

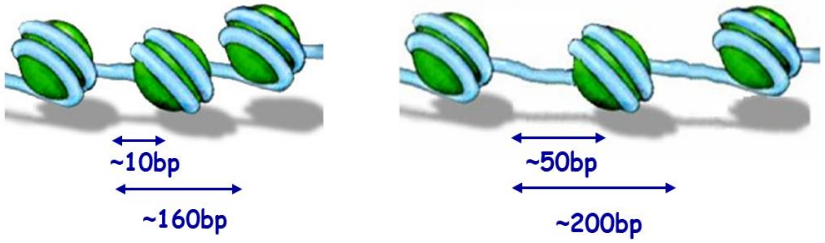

Fig. 5. Telomeres, generally considered heterochromatic, have an altered spacing between nucleosomes, which is shorter (160 bp) than in the bulk chromatin (200 bp) (Makarov et al., 1993).

Mammalian telomeres are further characterized by an hypoacetylated state of H3 and H4, (Benetti et al., 2007a) that are typical heterochromatic marks necessary for preservation of healthy telomeres. For example, hypoacetylation of lysine 9 and 56 of histone H3, properly maintained by SIRT6, is essential for a correct telomere capping (Tennen et al., 2011).
However, most evidences leading to the assumption that telomeres are heterochromatic, are principally based on data obtained on mouse telomeres (Schoeftner and Blasco, 2010). Several studies showed that the epigenetic status of human telomeres is less defined. Unexpected low levels of H3K9me3 were found at telomeres in

human fibroblasts (O'Sullivan et al., 2010), in human CD4C T-cells (Rosenfeld et al., 2009), and in nine human cell lines of different origin (Ernst et al., 2011). Recently, from the analysis of multiple ChIP-seq experiments carried out in several human somatic cells, it emerged the presence of euchromatic markers at telomeres, such as H4K20me1 and H3K27ac, and the lack of enrichment of H3K9me3 (Cubiles et al., 2018). Conversely, enrichment of H3K9me3 at telomeres has been found in U2OS, an ALT positive human cell line (Cubiles et al., 2018). At present, the definition of the epigenetic state of human telomeres is still an open question.

- **Telomeric nucleosome**

Telomeric nucleosomes are characterized by a lower stability with respect to bulk nucleosomes, with the same probability of assembly all along the telomere (Cacchione et al., 1997; Filesi et al., 2000; Rossetti et al., 1998). This is a sequence-dependent feature, since TTAGGG repeats are out of phase with the 10 bp DNA repeat in the nucleosome. The low thermodynamic energy required to slide from one position to another (Filesi et al., 2000) makes telomeric nucleosomes intrinsically mobile (Galati et al., 2013; Pisano et al., 2007). Recently, it has been obtained a 2.2 Å crystal structure of a telomeric nucleosome core particle (Telo-NCP), wrapped around by 23 TTAGGG repeats, which confirmed the features emerging from the *in vitro* studies have demonstrated new precious information about telomeric nucleosome features (Soman et al., 2020).
These characteristics may be crucial for telomere functions, such as inhibition of DDR pathways, dynamic regulation of epigenetic states, chromatin remodeling and maintenance of genomic integrity.

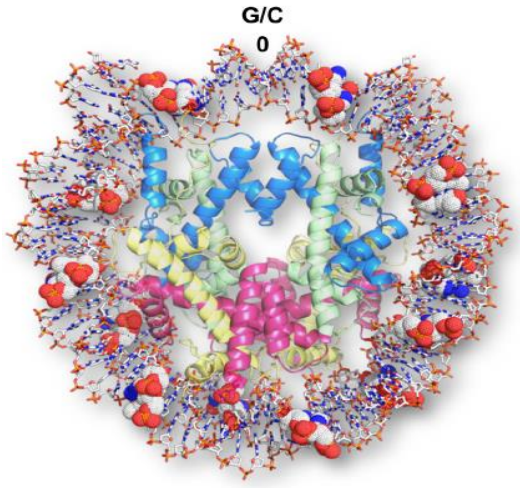

Fig. 6. Structure of the telomeric nucleosome core particle at 2.2 Å resolution. The histone octamer is painted in blue, green, yellow and red (H3, H4, H2A and H2B, respectively) and the base steps at minor groove pressure points are shown as space filling dots (Soman et al., 2020).

- **Nucleosome -Shelterin interplay**

It is now well established that nucleosomes and Shelterin co-exist at telomeres (Tommerup et al., 1994), but how nucleosomes are positioned along the chromosome ends and how they interact with the Shelterin complex it is not yet well defined.
It is worth noting that, beyond the presence of Shelterin, there is the documented presence of sub-complexes involving fewer shelterin members at telomeres (Giraud-Panis et al., 2010) and that this variegated composition reflects the dynamics in their binding on telomeric DNA. By FRAP assays it has been reported that binding of TRF1 and TRF2 to telomeres is highly dynamic (Mattern et al., 2004), whereas nucleosomes are stable structures with a very low turnover (Phair et al., 2004).
These and other evidences even a complex interplay between TRF1, TRF2 and nucleosomes on telomeric DNA. Through a gel mobility

shift assay and DNase I footprinting *in vitro* studies it has been demonstrated that TRF1 is able to bind to its target sequence on nucleosome forming a stable ternary complex, shaping telomeric chromatin and nucleosome mobility but without provoking octamer dissociation from DNA (Galati et al., 2006).
TRF1 is also able to induce sliding of a telomeric nucleosome (Pisano et al., 2010) and to stably bind naked DNA adjacent to a nucleosome (Galati et al., 2015). On the contrary, TRF2 binding to telomeric DNA is hampered by nucleosomes (Galati et al., 2015).
Moreover, Atomic Force Microscope (AFM) studies reveal the formation of more compacted nucleosome structures in presence of TRF2 (Baker et al., 2009; Pisano and Gilson, 2019) Nevertheless, overexpression of this Shelterin subunit *in vivo* augments the spacing between telomeric nucleosomes (Galati et al., 2012).
Despite the substantial number of evidences of how these proteins can affect chromatin regulation (Galati et al., 2015; Galati et al., 2006), MNase digestions performed in absence of TRF1 and TRF2 displayed no differences in the nucleosome spacing compared to WT, even in telomere deprotection conditions (Wu and de Lange, 2008). Further evidences are needed to clarify the involvement of Shelterin components in the regulation of telomeric chromatin.

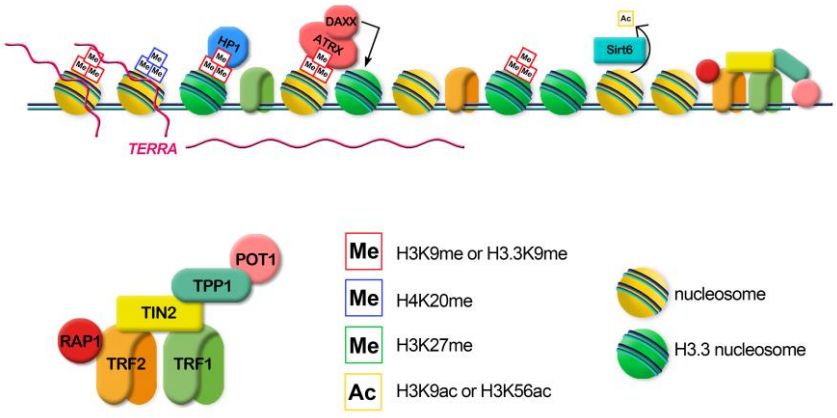

Fig. 7. Scheme of telomeric chromatin organization (Cacchione et al., 2019).

- **Histone variant H3.3**

Telomeric chromatin is enriched in the H3 histone variant H3.3 (Goldberg et al., 2010). This variant is constitutively expressed during the cell cycle, and is coded by two genes: *H3F3A*, located on chromosome 1, and *H3F3B* situated on chromosome 17. Unlike the canonical histones, these genes contain intronic sequences, the RNA have a poly-A tail and have different 5'-UTR (Frank et al., 2003).
H3.3 differs from its canonical counterparts, H3.1 and H3.2, in only five and four aminoacids, respectively (Fig. 8) (Filipescu et al., 2013).

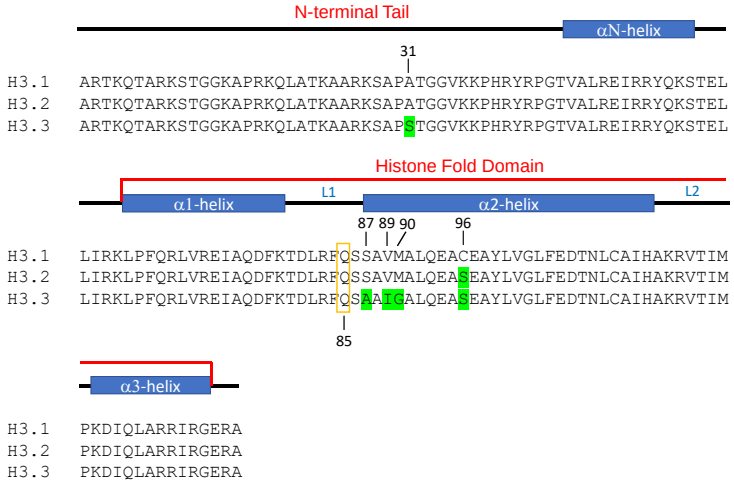

Fig. 8. Schematic view of the amino acid difference between canonical H3 (H3.1/H3.2) and histone variant H3.3

In particular, three of the five residues, ala87, ile89 and gly90 are crucial for recognition by the two complex that mediate its deposition: the histone chaperone complex ATRX/DAXX, which promotes its deposition at telomeres, pericentromeres, at imprinted genes and interstitial heterochromatic sites, and the histone chaperone HIRA complex, which deposits H3.3 at actively transcribed genes (Goldberg et al., 2010; Wong et al., 2010). These

specific deposition mechanisms indicate that H3.3 has multiple and distinct functions (fig. 9).

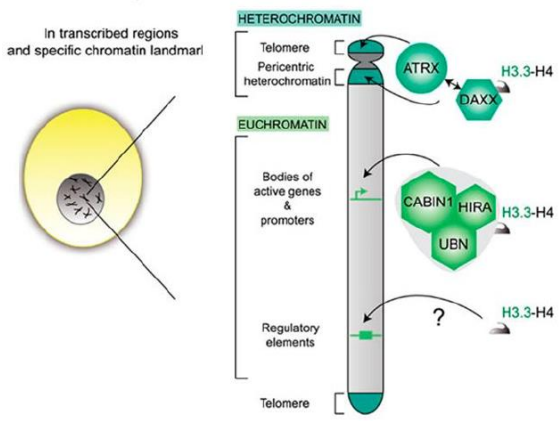

Fig. 9. H3.3 enrichment along the chromosome. In mammalian cells, H3.3 is found enriched both in highly transcribed genes and in heterochromatic regions. Deposition of this histone variant in the body and at promoters of active genes is mediated by HIRA, whereas the accumulation at telomeres and pericentromeres is exerted by ATRX/DAXX. Adapted from (Szenker et al., 2011).

Recently, it has been demonstrated the involvement of PML in H3.3 loading in the genome. These studies show that in mouse fibroblasts, PML depletion shifts the loading balance of the histone variant from the open chromatin to heterochromatic regions, such as telomeres and pericentric repeats (Spirkoski et al., 2019).
This broad range of functions could be explained, at least in part, by the different turnover rates along the genome, where promoters have a rapid turnover, gene bodies would be characterized by an intermediate turnover and the heterochromatic regions would display a slow rate.
The enrichment of H3.3 at telomeres is crucial for proper formation of telomeric chromatin. The presence of H3.3 at chromosome ends is associated with heterochromatin establishment, even though the

role of H3.3 at human telomeres still need to be explored, also because most of studies were carried out on mouse embryonic stem cells (mESCs) (Udugama et al., 2015) and mouse embryonic fibroblasts (MEFs) (Spirkoski et al., 2019).
Loss of H3.3 in mESCs leads to reduction of H3K9me3, H4K20me3 and ATRX at telomeres, followed by an increase in telomeric transcription, showing that the octamer with this variant is crucial for trimethylation of K9 and the telomeric heterochromatin establishment (Udugama et al., 2015). The presence of heterochromatic marks helps the structural integrity of telomeres, as shown in mice deleted for several DNA methyl-transferases (SUV39H1/2, SUV420H1/2, DNMT3A/B, and DNMT), which presents dysfunctional telomeres, aberrant telomere length and chromosomal instability (Benetti et al., 2007b; Garcia-Cao et al., 2004). Finally, a specific H3.3 PTM (phosphorylation at serine 31) is important for cell survival in ALT cancer cells and for telomere stability in mESCs (Chang et al., 2015; Wong et al., 2009).

HOW TELOMERIC PLAYERS MODIFY CHROMATIN LANDSCAPE: EPIGENETIC DEFECTS AT TELOMERES IN CANCER

H3.3 and cancer

In the last few years recurrent histone genes mutations have been reported in several cancers, with a prevalence of paediatric tumors. The mutant histones have been called "oncohistones", indicating mutant histones which have oncogenic features (Mohammad and Helin, 2017). So far, these mutations affect only three residues of the H3 histone, K27, G34 and K36 (Schwartzentruber et al., 2012), and show a dominant effect. Strikingly, most of these oncogenic mutations occur in H3.3. The expression of these oncohistones, even in heterozygosity (being mainly dominant mutations), heavily alters the global chromatin landscape, but the molecular mechanism is still unclear. Interestingly, oncohistone mutations are variant-specific, residue-specific and occur at high frequency, but in different cancer types and locations: histone H3K27M and G34R/V are usually found in paediatric brain cancers (Fontebasso et al., 2014; Mackay et al., 2017), whereas H3K36M and G34W/L mutations respectively occur in paediatric chondroblastoma and giant cell tumor of bone (Behjati et al., 2013). The highest frequency of H3.3 mutation has been found in chondroblastoma, with a 95% frequency of H3.3K36M (88% *H3F3B*, 7% *H3F3A*), whereas in giant cell tumors of the bone H3.3G34W/L mutation frequency is of 94% (*H3F3A*, 92% G34W, 2% G34L). Very high is also the frequency of K27M mutation in diffuse intrinsic pontine glioma (DIPG) (93%, *H3F3A*), which is present, even if at lower frequency, also in the canonical counterpart H3.1 and H3.2 (Mohammad and Helin, 2017; Nacev et al., 2019).

Notably, *H3F3A* and *H3F3B* have different untranslated regions, and, consequently, a different post-transcriptional regulation; in fact, *H3F3A* is characterized by a more uniform expression, differently from the *H3F3B* expression which is more differentiated

across tissues and this diversification seems to be recapitulated also in the occurrence mutation of the two genes: for example, K27M and G34R/V are present only at *H3F3A* gene (Mohammad and Helin, 2017).

- H3K27M

H3.3K27M mutation is abundant in the midline and pons, accounting for 63.0% DIPG and 59.7% non-brainstem midline tumor. This group is characterized by a shorter overall survival (median 11 months) (Mohammad and Helin, 2017).
H3K27M mutation acts as an inhibitor of EZH2, a methyl-transferase of PRC2, which leads to the loss of transcriptional silencing though an augmented levels of the acetylation of the histone H3K27, and at same time, heavily reduction of H3K27me3 (Jiao and Liu, 2015; Venneti et al., 2013).
However, the missense mutation of H3.3 is not sufficient to drive tumorigenesis (Schwartzentruber et al., 2012), but the combination with p53 depletion inducing diffuse tumorigenesis in both hindbrain and forebrain, while ATRX depletion is correlated with more circumscribed tumors (Pathania et al., 2017).

- H3K36M

As for H3K27M, it was found global loss of di-methylation and tri-methylation all over the genome, principally in chondroblastoma; in this case, mutation of K36M suppresses the enzymatical activity of NSD2/MMSET, that catalyzes mono- and di- methylation of H3K36, and of SETD2, which trimethylates K36 residue (Fang et al., 2016; Yang et al., 2016). This particular modification is essential for recruitment of Dnmt3b on actively transcribed genes, which exerts its role by preventing spurious transcription through methylation of the genes (Schwartzentruber et al., 2012). At least in part, K36M mutations drive tumorigenesis by altering the expression of cancer-associated genes (Zhang et al., 2017).

- H3G34R/V

The H3G34R/V mutations occur in paediatric non-brainstem high-grade gliomas (HGGs), preferentially in *H3F3A* gene, and R is a more common mutant than V (Nacev et al., 2019).
Even though G34R/V mutations do not directly occur at a site of post-translation modification, they affect the residue H3K36 that is close on the H3 tail,, which can be mono, di-, and tri-methylated or acetylated in association with transcriptionally active or silenced chromatin. Noteworthy, diffuse glioma shows a prominent hypomethylation at chromosome ends (Bender et al., 2013; Schwartzentruber et al., 2012).

- H3.3G34W

Also in this case, the mutation is defective for SETD2-mediated methylation, but co-occurs with augmented levels of H3K27me3 and reduction of H3K27ac and H3K9me3 (Fang et al., 2018).
The expression of this mutant leads to alterations in splicing, transcription and using of alternative start sites to promote cellular growth (Lim et al., 2017).
Mutations of other genes co-occurred with these H3.3 mutations, in particular the inactivating mutations of the ATRX and DAXX genes, which correlate with mutations of K27 with a variable percentage across studies (30-60%). ATRX mutations frequently arise with G34R/V histone mutations, with recorded co-mutation rates ranging from 75 to 100% in the larger cohort of GBMs (Schwartzentruber et al., 2012).
To summarize, the co-presence of H3.3 missense dominant mutations, recurrent inactivation of ATRX/DAXX and ALT phenotype development suggests a possible link between all these elements, and a deeper investigation could bring new important information about the mechanism of how these cancers arise.

Tumor	Mutation	Histone subtype	Affected gene	Frequency	Codon wild type (mutated)
DIPG	K27M	H3.3	H3F3A	Up to 93%	AAG (ATG)
		H3.1	HIST1H3B	Up to 31%	AAG (ATG)
			HIST1H3C	<3%	AAG (ATG)
		H3.2	HIST2H3C	<2%	AAG (ATG)
	K27I	H3.3	H3F3A	<1%	AAG (ATT)
Non-DIPG pHGG	G34R	H3.3	H3F3A	12%–14%	GGG (CGG/AGG)
	G34V	H3.3	H3F3A	<2%	GGG (GTG)
GCTB	G34W	H3.3	H3F3A	92%	GGG (TGG)
	G34L	H3.3	H3F3A	<2%	GGG (TTG/CTG)
Chondroblastoma	K36M	H3.3	H3F3B	88%	AAG (ATG)
			H3F3A	7%	AAG (ATG)

Fig. 10. Summary of the major dominant point mutations of H3.3 in pediatric tumors, with frequency of insurgence (Mohammad and Helin, 2017).

TRF2 extratelomeric functions and cancer

It has been demonstrated that TRF2, beyond its telomeric functions, has also extra-telomeric roles. Indeed, TRF2 can regulate the transcriptional activation by occupying a set of ITS throughout the human genome, referred to as interstitial telomeric sequences (Simonet et al., 2011), or through the binding of REST, that regulates neural differentiation (Kwon et al., 2012).
TRF2 is also involved in DNA damage response, where it has been found associated with DSBs (Bradshaw et al., 2005).
Moreover, several ChIP-seq assays performed in HT1080 fibrosarcoma cells displayed the presence of thousands TRF2-binding sites along the genome, enriched in potential G-quadruplex forming DNA sequences. TRF2 associates with several of these validate G4s in gene promoters, affecting their epigenetic state and expression (Mukherjee et al., 2019).
Also pericentromeric satellite III sequences are bound by TRF2, in particular during S phase, where the protein acts as a sort of overseer, ensuring the correct progression of the replication fork through RTEL1 recruitment, a helicase necessary for resolution of G4s (Mendez-Bermudez et al., 2018).
This wide diversification of activities exerted by TRF2 is principally due to its N-terminal basic domain rich in glycine and arginine residues, which allows TRF2 association to DNA in a sequence-independent manner (Deng et al., 2009; Fouche et al., 2006; Poulet et al., 2009).
In the last past years, growing evidences have described the involvement of this Shelterin component in cancer development. Indeed, TRF2 has been found upregulated in many tumors (Biroccio et al., 2013; Diala et al., 2013; El Mai et al., 2014; Munoz et al., 2005; Nakanishi et al., 2003). Through an extrinsic mechanism which involves NK cells, TRF2 is able to localize at an ITS contained in a gene coding for the heparan sulphate 3 – sulfotransferase (Cherfils-Vicini et al., 2019) which is involved in regulating NK cell recruitment/activation at the tumor site with an

impact on tumor take/growth. Other genes regulated by TRF2 are PDGFRβ (El Mai et al., 2014) and p21 (Hussain et al., 2017). To date, many studies documented the correlation between cancer development and alterations (or mutations) not only in TRF2, but also in the other Shelterin components.

For example, Rap1 associates to both subtelomeric related genes and genes linked to metabolic regulation, cell adhesion and cancer.

Dysfunctional telomeres were documented in patients in early stage of chronic lymphocytic leukemia (Lin et al., 2010), and telomere to telomere fusions were present in patients in late stage of the disease (Augereau et al., 2011). In agreement with telomeric defects, the researchers detected decreased levels of TRF1, RAP1 and POT1 (Poncet et al., 2008) TIN2 and TPP1 (Augereau et al., 2011).

POT1 and RAP1 mutations have been found also associated with familial melanoma, familial glioma, Li-Fraumeni-like syndrome, mantle cell lymphoma and parathyroid adenoma (Cacchione et al., 2019).

These evidences demonstrate a clear implication of Shelterin alterations in establishment of telomeric instability, and an involvement in cancer development. However, the mechanistic insights of shelterin alterations in cancer development still need to be clarified.

SIRT6 and cancer

SIRT6, a member of the mammalian sirtuin family of Nad^+-dependent histone deacetylases, is a well-known chromatin remodeling factor implicated in telomere integrity and homeostasis (Michishita et al., 2008). SIRT6 is a complex enzyme with multiple substrates and catalytic activities, as deacetylation of both histones and non-histone proteins; deacetylation of long-chain fatty acyl groups and mono-ADP-ribosylation activity (Kugel and Mostoslavsky, 2014; Mao et al., 2011; Rezazadeh et al., 2020; Rezazadeh et al., 2019). At chromatin level, SIRT6 binds nucleosome (Liu et al., 2020) and deacetylates the histone H3 on acetylated K9, K56 (Michishita et al., 2008; Yang et al., 2009) and the more recently identified K18 and K27 residues (Tasselli et al., 2016; Wang et al., 2016), causing the repression of many genes differently involved in inflammation, aging, genome stability, metabolic pathways and telomere integrity (Jia et al., 2012; Liu et al., 2020; Mei et al., 2016).

At telomeres, SIRT6 prevents impaired silencing of telomere-proximal genes (Tennen et al., 2011); allows the proper replication of chromosome ends through deacetylation of H3K9 and H3K56 during S-phase (Michishita et al., 2009) and ensures the correct recruitment of the WRN helicase. Loss of SIRT6 brings to formation of dysfunctional telomeres, with end to end fusions and stochastic replication-associated telomere sequence loss, in a phenotype Werner syndrome-like, leading to cell senescence and genomic instability (Michishita et al., 2008; Yang et al., 2009).

The role of SIRT6 in cancer is controversial. In some tumors, high levels of this sirtuin are correlated with poorer outcomes (Huang et al., 2017; Khongkow et al., 2013; Marquardt et al., 2013). In other cancers, including colorectal cancer (CRC), low levels of SIRT6 are associated with its tumor suppressive activity (Kugel et al., 2016; Liu et al., 2018).

Recently, it has been reported that TRF2, one component of the Shelterin, is a substrate of SIRT6. The telomeric protein undergoes

to the ubiquitin-dependent proteolysis upon SIRT6-mediated deacetylation of TRF2 lysine residues leads to ubiquitin-dependent proteolysis. This process is activated upon DNA damage and subsequent DDR. Of note, in a cohort of CRC patients, an inverse correlation between SIRT6 and TRF2 protein expression levels have been found (Rizzo et al., 2017). This finding suggests the hypothesis that an impairment of TRF2 degradation, as a consequence of SIRT6 low levels, could be one of the mechanisms contributing to the increased dosages of TRF2 observed in many human malignancies. In addition to protein stability, whether SIRT6 could also affect the binding affinity to DNA of TRF2 (and eventually of other Shelterin factors) remains to be fully investigated.

AIMS OF THE WORK

Despite the crucial role that telomeres play in assuring chromosome stability and their involvement in cancer development, little is known about the epigenetic alterations of telomeric chromatin that affect telomere protection (Cubiles et al., 2018; Galati et al., 2013). Some of the most used approaches to study chromatin structure and function - including ChIP, ChIP-seq, MNase-seq – are less informative when applied at telomeres. This is mainly due to the complex nature of human telomeres, characterized by high length heterogeneity and low sequence complexity. Consequently, we have only limited information on nucleosome spacing or on histone composition and modification, while it is quite impossible to distinguish nucleosomes close to the subtelomeres from those at the very end of the chromosome.

In this thesis, we focus on two poorly characterized aspects of telomeric chromatin involved in telomere dysfunctions and tumor establishment. The first is the role played by SIRT6 deacetylase. It has been previously shown that SIRT6 interacts with TRF2 and that DNA damage stimulates the increase of this association. In particular, there is an increase of TRF2 deacetylation by SIRT6 upon DNA damage, with a consequent increase of TRF2 degradation (Rizzo et al., 2017). Interestingly, an inverse correlation between TRF2 and SIRT6 expression has been found in a cohort of CRC samples, suggesting the possibility that the oncosuppressive functions of SIRT6 can result at least in part in its ability to regulate TRF2 protein stability. It is known that alterations in telomeric chromatin and in telomere stability are often associated with cancer, but the molecular details of this association are still largely unknown. In order to answer, at least in part, to this issue, we addressed the functional interplay between TRF2 and SIRT6 in genomic stability and tumor formation, in order to identify novel effective anticancer strategies.

The second aspect is the role played by the histone variant H3.3 at telomeres. To address this issue, we developed new tools and a

different approach to map H3.3 positions at telomeres. First, we set up a method to chemically cleave nucleosomal DNA at 25 bp from the dyad axis of H3.3 containing nucleosomes. Then, to overcome the difficulties generated by the uniformly repeated telomeric sequence, we developed a strategy to map nucleosome positions using subtelomeric sequences as starting point. To characterize the fragments of different length emerging from MNase or chemical cleavage, we took advantage of Oxford Nanopores sequencing, a Technology that can handle very long fragments and does not require any amplification step.

RESULTS

1.SIRT6 is involved in stabilizing the binding of TRF2 to chromatin

It has been previously shown that the binding of TRF2 to nucleosomal telomeric DNA is hindered by the presence of nucleosomes. Furthermore, also TRF2 binding affinity for naked DNA is reduced by the presence of an adjacent nucleosome (Galati et al., 2015). Since it has been shown that SIRT6 binds to nucleosomes deacetylating H3 (Liu et al., 2020) and interacts with TRF2 (Rizzo et al., 2017), we asked whether SIRT6 could affect the binding of TRF2 to the nucleosome. To this aim, we used a particular DNA sequence, Tel2-601-Tel2, composed by the 601 fragment, a 147 bp long DNA fragment having high affinity for the histone octamer and forming a very stable reconstituted nucleosome (Lowary and Widom, 1998), flanked by two telomeric repeats at each side.
We reconstituted the Tel2-601-Tel2 DNA fragment into a nucleosome by salt dilution and incubated the reconstituted nucleosome with different amounts of TRF2 and SIRT6. Fig. 11 shows the binding of TRF2 to nucleosomes formed on Tel2-601-Tel2. At increasing TRF2 concentration the unbound nucleosome band (NCP) decreases and two shifted bands appear, corresponding to the binding of two TRF2 dimers to the two telomeric binding sites (Fig. 11, lanes 2-4). SIRT6 binds to the nucleosome forming a ternary complex with the nucleosome (Fig.11, lane 5). The addition of SIRT6 to the TRF2/nucleosome binding reaction causes the shifting of the complex and the disappearing of the unbound nucleosome (Fig. 11, lane 6-8).

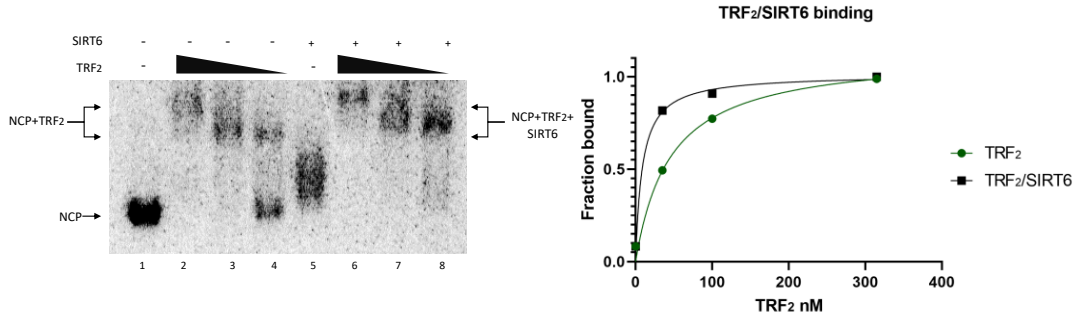

Fig. 11. TRF2 binding to nucleosomal telomeric sequences is stabilized by the presence of SIRT6. Gel mobility-shift assay NCPs formed on Tel2-601-Tel2 were incubated with decreasing amounts of TRF2 (lane 2-4 and 6-8, 35, 100 and 350 nM), and with the same quantity of SIRT6 (lane 5-8, 500 nM). Samples were separated on an 8% acrylamide gel.

We then analyzed whether SIRT6 affects TRF2 binding to chromatin. We performed a chromatin extraction in HCT-116 cell line depleted for SIRT6 (fig. 12a).
In the absence of SIRT6 we measured a substantial reduction of TRF2 in the chromatin extract, suggesting that SIRT6 is important to stabilize TRF2 binding to chromatin. This finding is even more significant since SIRT6 depletion results in an increased TRF2 expression (Rizzo et al., 2017). Conversely, depleting TRF2 has no effect on SIRT6 binding to chromatin (fig 12b). As additional control, since it has been shown that DNA damage increases SIRT6 recruitment to the chromatin, cells were treated with 1 μM of Camptothecin (CPT) for 2 hours. DNA damage enhances SIRT6 binding to the chromatin as expected, but this augmented association is not affected by TRF2 interference.
Collectively, these data suggest that SIRT6 is involved in the stabilization of TRF2 binding to chromatin.

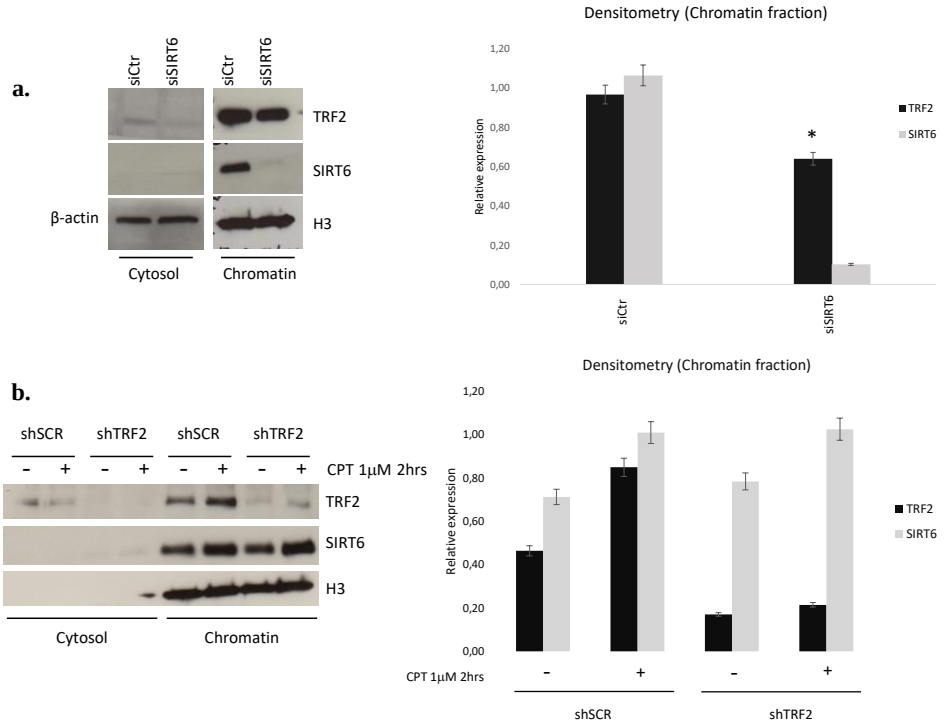

Fig. 12. Chromatin extraction from colon cancer cell line. (a) TRF2 association to chromatin significantly decrease upon SIRT6 depletion, whereas (b) SIRT6 association to chromatin does not change upon TRF2 depletion. H3 histone has been used as a normalizer and control of the extraction protocol.

2. TRF2 delocalizes from heterochromatic regions upon SIRT6 silencing

Since recent findings demonstrated the presence of TRF2 also at pericentric regions (Mendez-Bermudez et al., 2018), and that SIRT6 specifically deacetylases lysine 18 of histone H3 (H3K18) at pericentromeres (Tasselli et al., 2016), we asked whether SIRT6 may affect TRF2 binding at different genomic locations. We down-regulated SIRT6 expression in HCT116 cells by RNA interference (fig. 13a) and performed a ChIP experiment with an antibody recognizing TRF2. As a control, we also immunoprecipitated using an antibody against H3K18ac, which is a main target of SIRT6 deacetylation activity. Fig. 13b shows a dot-blot hybridized with probes specific for telomeric sequences, satellite DNA and Alu sequences. The hybridization with the telomeric probe shows a significant decrease of TRF2 binding at telomeres (quantified in fig. 13c). Upon SIRT6 depletion, TRF2 binding decreases at pericentromeres as well. Acetylation of H3K18 at pericentromeres increases upon SIRT6 depletion, confirming previous reports (Tasselli et al., 2016). Instead, at telomeres H3K18ac slightly increase upon SIRT6 depletion, a finding that requires further investigation.

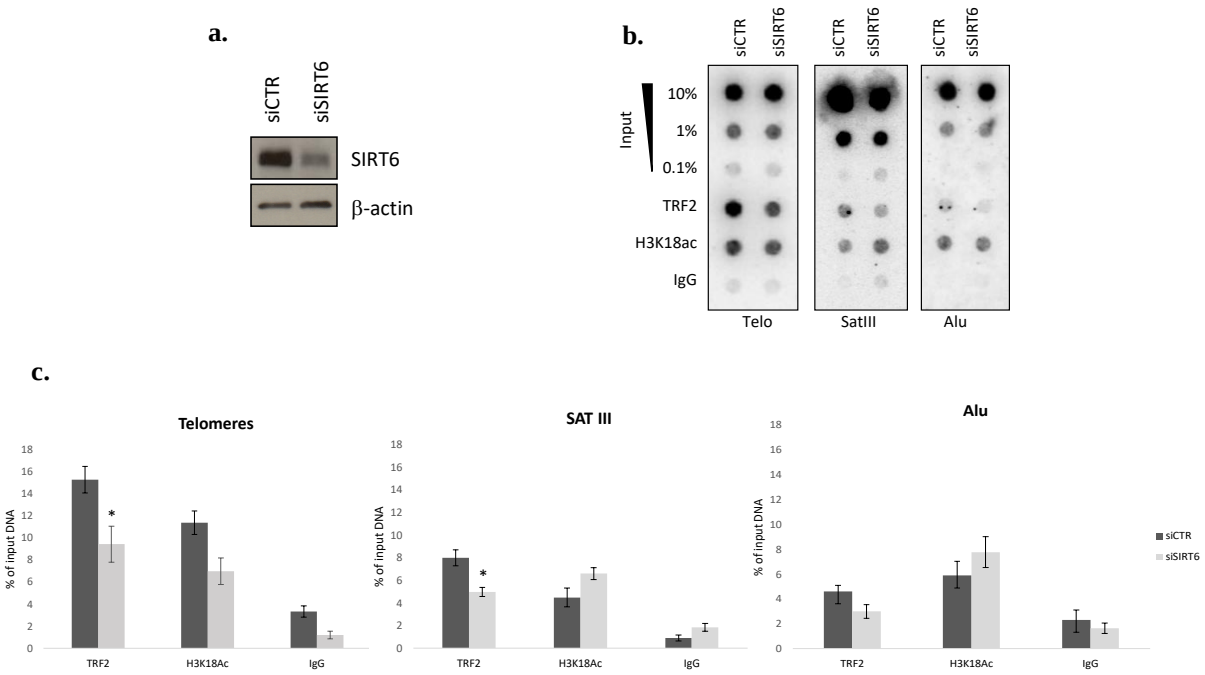

Fig. 13. ChIP experiment on colon cancer cell line interfered or not for SIRT6. Inhibition of SIRT6 was checked by WB, as shown in (a). The crosslinked filter has been hybridized with a telo-probe, a sat III probe and an Alu probe (b). As a further control, H3K18Ac, which is a typical target of SIRT6, was immunoprecipitated. In (c) quantifications of ChIP experiment are reported. All data are shown as the mean +/- SEM of three separate experiments.

Then, we decided to study genome-wide the dynamics of TRF2 binding to chromatin upon SIRT6 depletion by a ChIP-seq analysis. The most relevant result emerging from ChIP-seq is the delocalization of TRF2 from repeated heterochromatic regions such as ALR/Alpha satellite repeats, LINEs and SINEs, and in general, from pericentromeric regions (fig. 14 and fig. 15). Strikingly, ChIP-seq analysis shows also several peaks gained upon SIRT6 depletion. In particular, many peaks gained correspond to gene promoters, even though also ALR/Alpha sequences and LINE/SINE sequences are listed too.

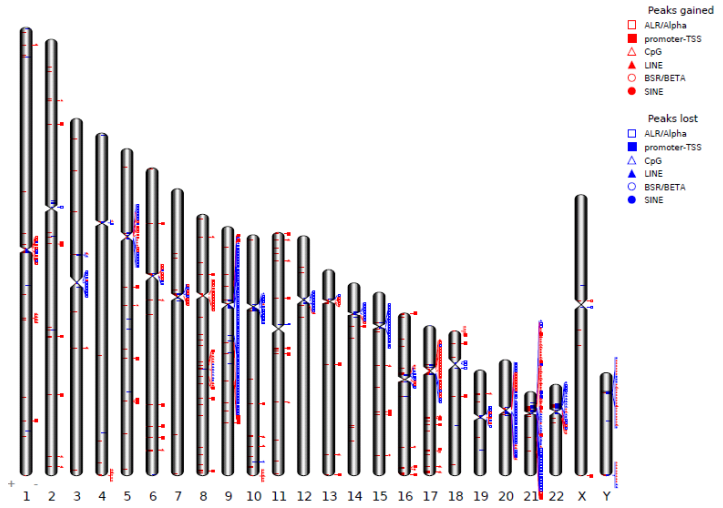

Fig. 14. The differential peak positions found for the TRF2 ChIP-seq were plotted along the human karyotype ($p<10^{-4}$). Blue positions represent the peaks lost in siSirt6 conditions compared to the Control, red positions represent the peaks gained. The 6 most common patterns found near the peaks were represented as symbols (squares, triangle, circles, full or empty). The motifs were identified during the annotation step of the ChIP-seq analysis by using the Homer tools suite. This drawing was made thanks to the tool Idiographica and by a home-made annotation script to add the motifs symbols onto the image.

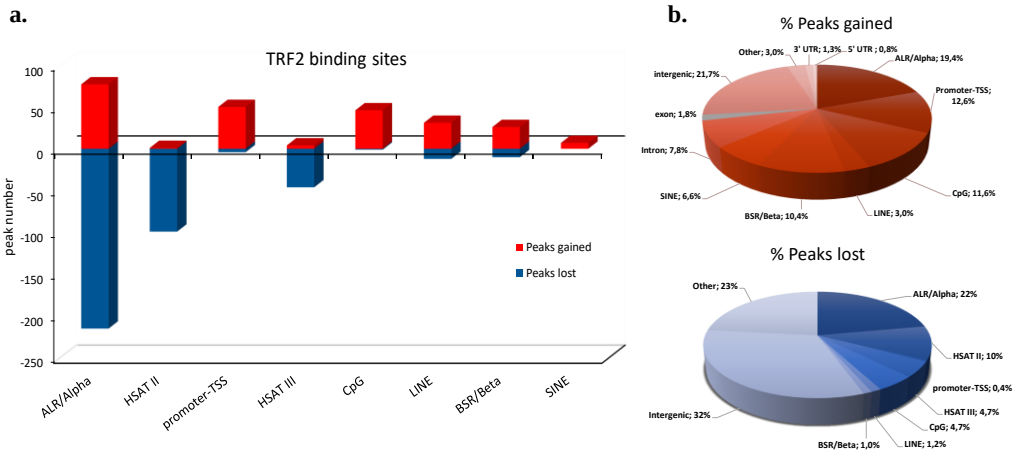

Fig. 15. Annotation of TRF2 ChIP-seq peaks (a) In blue are showed the lost peaks and in red the peaks gained. Pie charts in (b) represent the peak distribution across the genomic regions in percentage. The α-satellite, together with the HSAT II and III show the major loss of TRF2 binding. In SIRT6 silencing condition, several promoters acquire a significant increase of TRF2 binding.

The genome-wide peak profile analysis of TRF2 ChIP-seq reads allowed the identification of 88 genes among the gained peaks and 16 genes among the lost peaks in the SIRT6-KD samples compared to the control ones. Interestingly, many of the identified genes enriched in TRF2 when comparing SIRT6-KD *versus* control samples have been reported to have a role in tumorigenesis (i.e HBEGF, TOM1L1, TRAF6, PDP1, Fig. 16). This enrichment on gene promoters is also in accordance with the recent findings that put in evidence the involvement of TRF2 in regulation of gene expression in cancer cells. Further analysis will be necessary to verify the effect of the TRF2 binding on the transcriptional outcome of these genes.

Gene	Distance to TSS	Fold change
ARHGAP28	47	89,72
NME2	-61	60,92
CD151	-152	49,22
ANKRD20A4	-243	37,44
MOB4	-123	26,02
NUDT22	366	22,15
MCFD2	15	20,01
PCMT1	45	18,27
COBLL1	88	17,83
VPS36	58	17,34
UBR5	-291	17,33
CTNNAL1	-46	17,33
SEMA6A	26	16,46
DNAJA1	-183	16,39
TOM1L1	29	16,29
HBEGF	-57	16,06
F2R	77	15,87
RAD9A	-72	15,85
TRAF6	13	15,82

Gene	Distance to TSS	Fold change
FLOT1	-69	15,73
COX4I1	-58	15,45
SLC39A6	-26	15,45
MED23	-1	15,23
RRP15	-127	15,20
PAXBP1	-82	15,00
MRPL39	-91	14,88
SNX16	-174	14,74
IPO4	-22	14,73
FUT10	-74	14,63
FRA10AC1	-88	14,59
ABCA5	-118	14,48
ADAT2	4	14,08
TMEM255B	-23	14,07
THEM6	77	10,53
PDP1	-14	9,57
SNAPC5	-65	9,19
VPS9D1	-194	4,18

Fig. 16. Annotated list of the genes found enriched in TRF2 on promoters upon SIRT6 depletion. In bold are showed those promoters involved in tumorigenesis according to literature.

3. High Resolution mapping of H3.3 nucleosome positions in Human cells.

A novel method of high-resolution nucleosome mapping in *Saccharomyces cerevisiae* was developed by Widom and co-workers by introducing a cysteine at position 47 of histone H4 and successively performing a chemical reaction which cleaved DNA at the dyad axis of nucleosomes (Brogaard et al., 2012). Recently, a similar approach was used by the Henikoff and coworkers, who showed how mutating the glutamine residue at position 85 of histone H3 into cysteine can be used to accurately map nucleosome positions in budding yeast (Chereji et al., 2018). More in detail, this new cysteine close to the DNA minor groove is responsive to a chemical cleavage reaction in the presence of phenanthroline, copper and hydrogen peroxide. N-(1,10-phenanthroline-5-yl) iodoacetamide (Phe) is a sulfhydryl-binding copper chelating agent, that covalently binds cysteine thiolic group on H3Q85C and chelates a copper ion to DNA; the presence of hydrogen peroxide causes the hydroxyl radical-mediated cleavage of DNA where the copper ion is bound (fig. 17).
In a nucleosome containing two copies of the mutant histone, the reagents provoke a double-strand cleavage 25 bp apart from the nucleosome dyad axis; this means that a 51-bp DNA fragment is released and that the midpoint of this fragment corresponds to the precise nucleosome dyad position (fig. 18). Next-generation sequencing (NGS) of the 51 bp DNA library allowed the direct mapping of nucleosome positions along the genome (Chereji et al., 2018). The yeast H3 gene encodes for a H3.3-like protein (Elsaesser et al., 2010). Therefore, it is likely that introducing the same mutation (Q85C) in human H3.3 genes would result in a similar sensitivity to phenanthroline/copper/hydrogen peroxide treatment. Adapting the chemical cleavage to human H3.3 sounded like a solid approach to map H3.3-containing nucleosome positions.

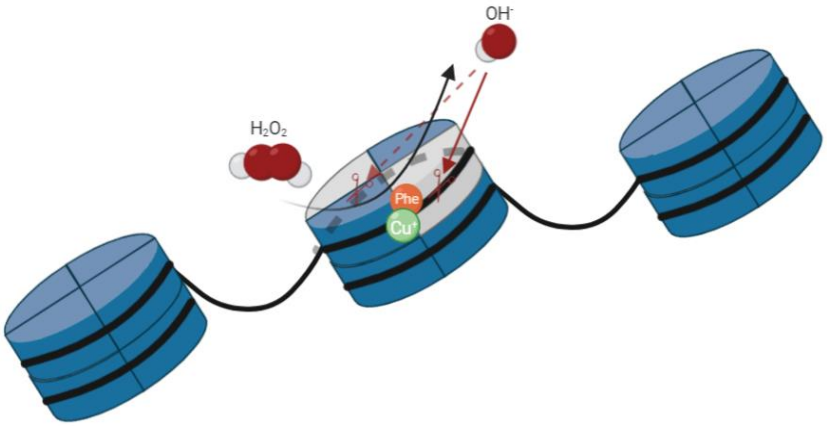

Fig. 17. The H3.3 histones are shown in white. N-(1,10-phenanthroline-5-yl) iodoacetamide (Phe) covalently attached to the residue H3.3Q85C, chelates a copper ion (Cu^{+}) to DNA; the presence of hydrogen peroxide causes hydroxyl radical cleavage of DNA where copper is bound.

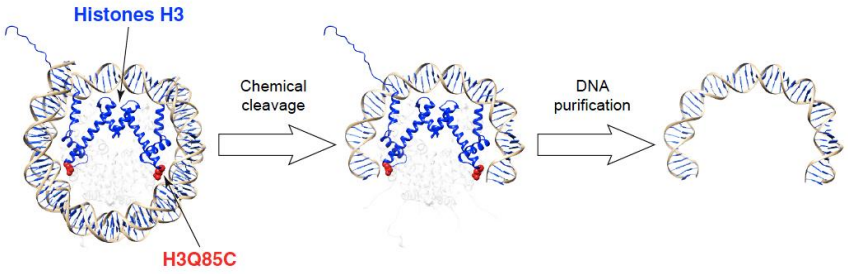

Fig. 18. Schematic representation of the phenantroline-driven chemical cleavage and release of 51-bp long DNA fragments. (Chereji et al., 2018)

4. The mutant histone H3.3Q85C is incorporated in chromatin in transgenic human cell lines

In order to set-up a H3.3-specific chemical cleavage mapping we first infected Hela cells and BJ-hTERT fibroblasts with lentivirus carrying the vector for the exogenous expression of the mutant H3.3 Q85C fused to a 3xFLAG peptide.
After puromycin selection, the expression of the exogenous H3.3 Q85C was checked by Western Blot by using an anti-FLAG antibody. As shown in fig. 19 the expression of the transgene is robust in BJ-hTERT cells, less strong in HeLa cells.

.

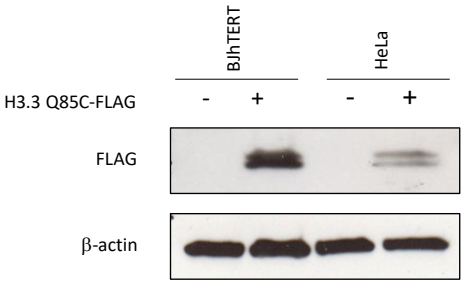

Fig. 19. Western blot with anti-FLAG antibody shows the expression of the H3F3AQ85C transgene in the infected BJ-hTERT and Hela cells. β-Actin is shown as a normalizer and loading control.

In order to ascertain the correct nuclear localization of the mutant protein, we immunostained cells with anti-FLAG antibody (fig. 20). A diffuse signal was evident in the nucleus of cells transfected with the H3Q85C transgene, indicating that the mutant protein was expressed and incorporated into chromatin. Merging of anti-FLAG with anti-TRF2 images confirmed also the presence of H3.3Q85C at telomeres.

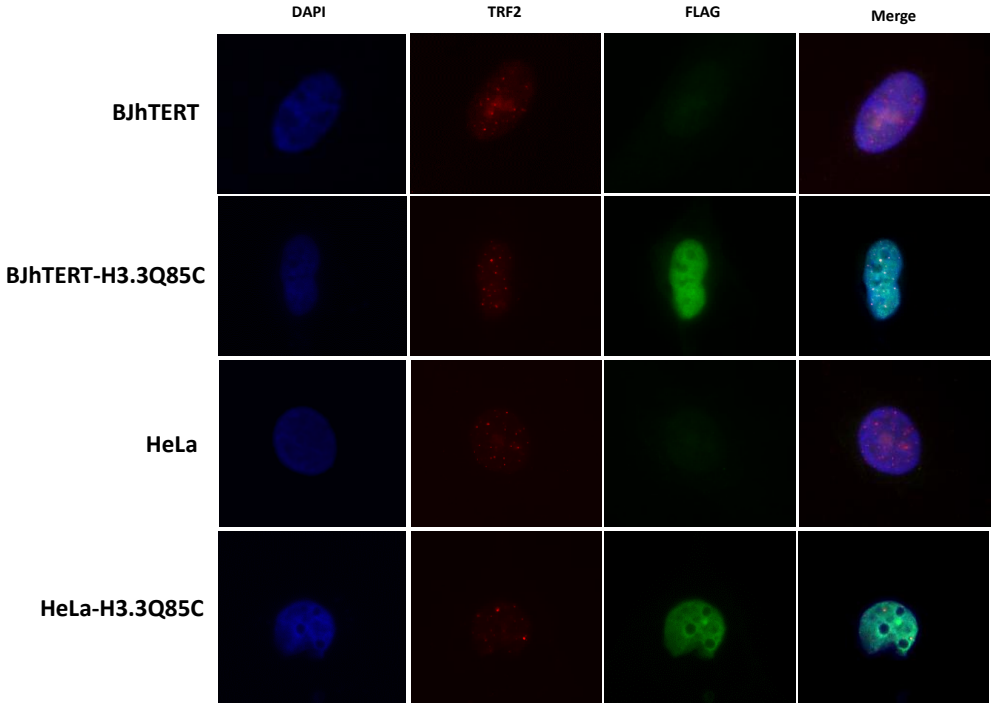

Fig. 20. Representative Immunostainings of Parental and infected BJ-hTERT and HeLa cells with a mutant H3.3Q85C, stained for nucleus (DAPI), H3.3Q85C (anti-FLAG) and a Shelterin component (anti-TRF2); Original magnification, 63x. Scale bar 50 µm.

As a further control, in order to verify the proper integration of the transgenic mutated histone variant in the histone octamer, we performed a chromatin extraction from BJ-hTERT and HeLa infected cells. As shown in fig. 21, western blot with FLAG antibody clearly shows that the mutant protein is present at chromatin but not in the cytosol. These data indicate that the transgenic H3.3Q85C is strongly expressed in our cell lines and correctly integrated in nucleosomes.

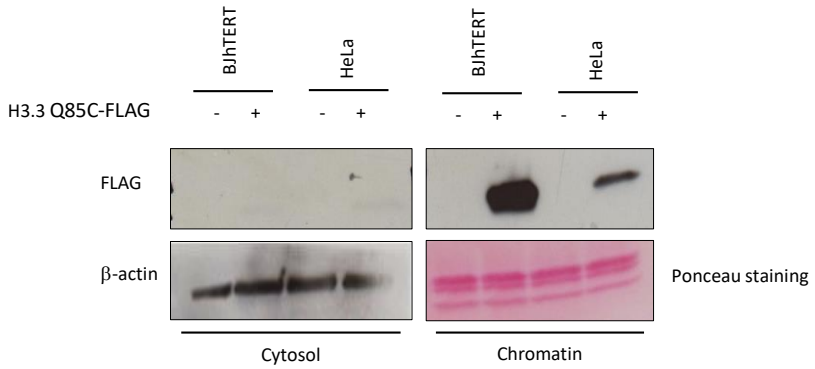

Fig. 21. Chromatin extraction from BJhTERT and HeLa cell line expressing H3.3Q85C-FLAG. Cytosol was normalized with actin antibody and chromatin with a Ponceau staining.

5. Genomic DNA of transgenic cell lines expressing H3.3Q85C is chemically cleaved

In order to assess that nucleosomes containing H3.3Q85C can be chemically cleaved, we treated transgenic cells with Phe/Cu/H_2O_2. The reactions were performed incubating cells in a medium containing 1.4 mM N-(1,10- Phenanthrolin-5-yl) iodoacetamide for 2 hours at room temperature. Then, 0.15 mM $CuCl_2$ and 6 mM of H_2O_2 were added to induce hydroxyl radical-mediated cleavage of DNA.

After treatment, genomic DNA was extracted and run on an agarose gel. Fig. 22 shows that in the presence of Phe/Cu/H_2O_2 genomic DNA from HeLa-H3.3Q85C cells is partially degraded with respect to the untreated control.

This result is in agreement with what expected from the chemical cleavage of nucleosomal DNA in H3.3Q85C-expressing cells. In dividing cells, H3.3 is present in about 20% of total nucleosomes (McKittrick et al., 2004) and the exogenous mutant gene only accounts for a fraction of total H3.3. Consequently, H3.3Q85C is distributed randomly and unevenly along the genome, which implies a pool of cleaved fragments of various length. For the same reasons, the 51-bp band characteristic of the chemical cleavage of H3Q85C in yeast (Chereji et al., 2018) is not visible; to release a 51-bp DNA fragment both H3.3 copies in a nucleosome must carry the Q85C mutation.

A small level of degradation is present also in genomic DNA from HeLa parental cells treated with Phe/Cu/H_2O_2, ascribable to non-specific cleavage by phenanthroline in linker DNA (Chereji et al., 2018). A higher level of genomic DNA degradation is evident in BJ-hTERT-H3.3Q85C treated with Phe/Cu/H_2O_2 (Fig. 23). This result is consistent with the higher expression of H3.3Q85C-FLAG in BJ-hTERT-H3.3Q85C with respect to HeLa-H3.3Q85C (see Fig. 19 and 21).

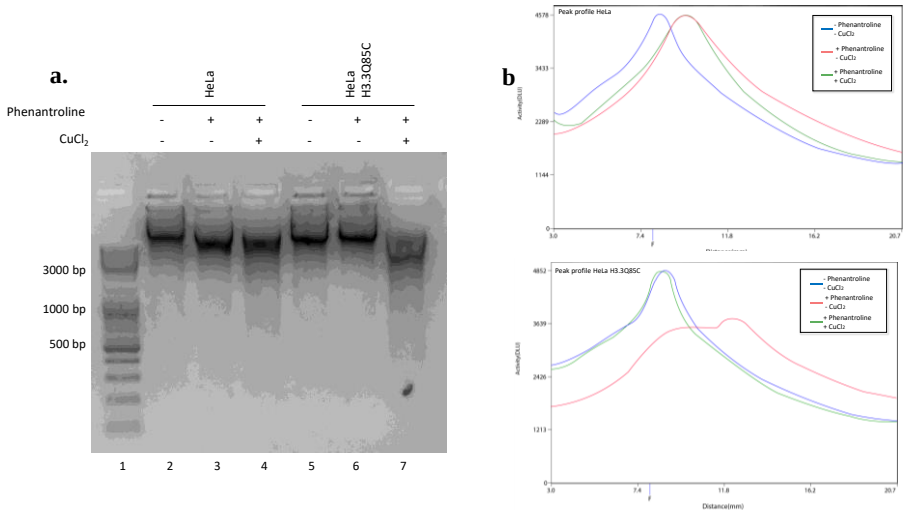

Fig. 22. Chemically cleaved genomic DNAs of treated cells resolved on agarose gel. **a)** Cleaved DNA from HeLa-H3.3Q85C cells yields a smear when treated with phenanthroline and copper (lane 7), unlike the untreated sample (lane 5) or the gDNA from the control parental HeLa cells, regardless of phenanthroline/copper usage (lanes 2-4). **b**) peak profiles of the chemical cleavage. The blue lines indicate control samples without phenantroline; in green are plotted samples with phenantroline without $CuCl_2$ and in red are indicated the samples with both reagents.

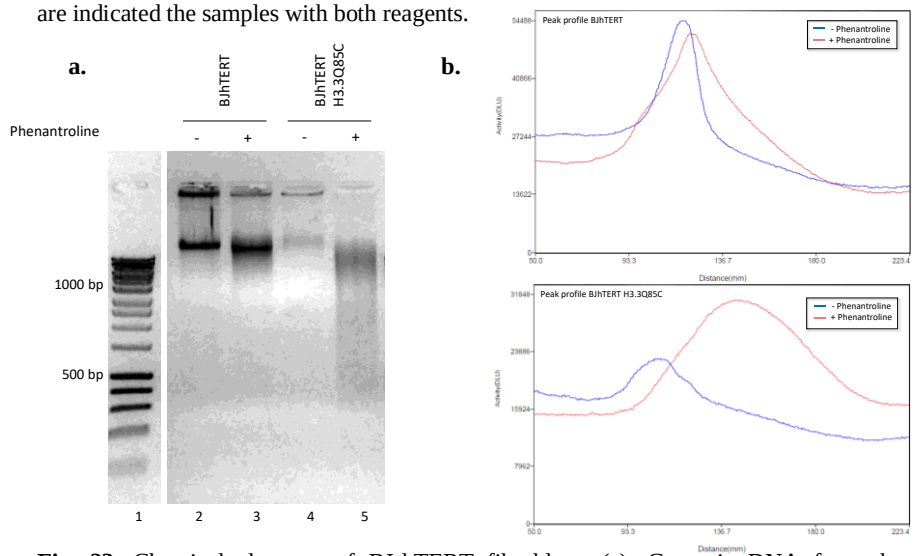

Fig. 23. Chemical cleavage of BJ-hTERT fibroblasts (a). Genomic DNA from the transgenic BJ-hTERT-H3.3Q85C cell line shows a general degradation (lane 5), which is instead absent in Phe- (lane 4) and in parental control (lanes 2-3). In (b) the peak profiles of the chemical cleavage. Blue: untreated samples; red: samples treated with phenantroline.

6. Strategy to map H3.3 nucleosomes at telomeres.

In order to map H3.3 positions genome-wide, the DNA fragments released by the chemical cleavage in BJ and HeLa cells transfected with H3.3 Q85C gene are too heterogeneous. The best strategy would be to increase the ratio H3.3Q85C/H3.3 wild type endogenous genes in order to obtain a 51 bp DNA library. However, the partial and random cleavage shown in Fig. 22 and 23 might represent the basis to obtain a map of H3.3 nucleosome positioning on telomeres. Few data are available about telomeric nucleosomal organization. Due to the uniformly repeated sequence, the only information emerging from classical MNase mapping studies was that telomeric chromatin has an unusual short spacing (Galati et al., 2012; Tommerup et al., 1994). It is still unknown whether the proximal part and the distal part of telomeres have different organizations, and consequently there are no data on H3.3 nucleosome positioning. For the same reasons, deep sequencing of the 51 bp DNA library derived from chemical cleavage could only give information on telomeric nucleosome occupancy, but not on telomeric nucleosome positioning. A strategy to infer nucleosome positions on a long-repeated sequence is to use adjacent DNA as starting mapping point: in the case of telomeres, subtelomeric sequences. Therefore, the random partial chemical cleavage shown in fig. 22 and in fig. 23, which could also be obtained by dosing phenantroline, and which releases longer fragments extending also on subtelomeric DNA, seems ideal to map telomeric H3.3 nucleosome positions (fig. 24). To complete our mapping strategy, we needed to be able to analyze and sequence the long DNA fragments released by the chemical cleavage. We decided to use an emerging sequencing technique that allows sequencing long DNA fragments, namely Oxford Nanopores sequencing.

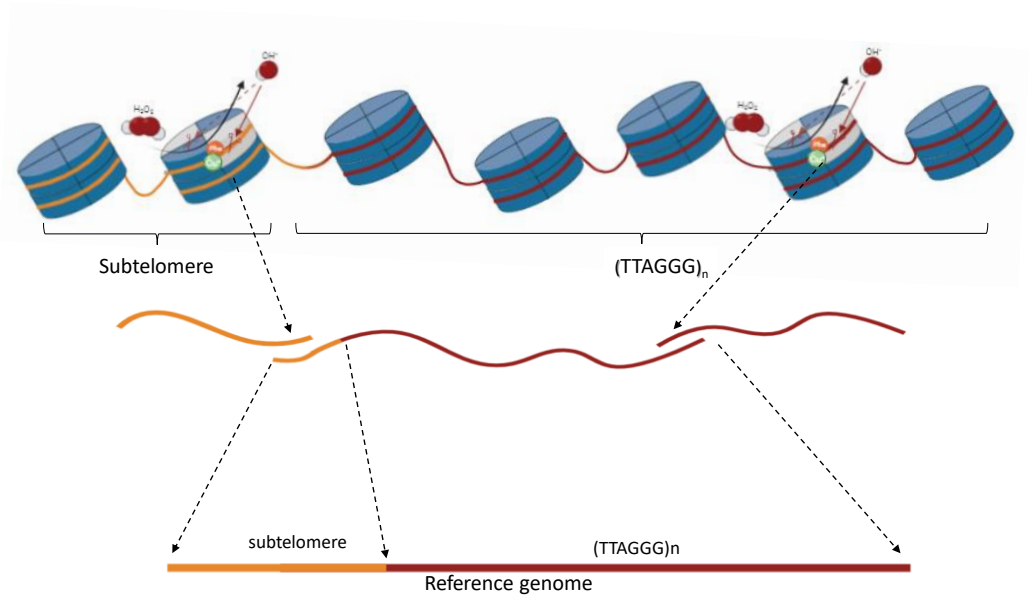

Fig. 24. Experimental design to chemically map nucleosomes on telomeres. Generation of long fragments that includes the unique Subtelomere sequences (in light yellow) in addition to telomeres (in red). The subtelomeres will be used to realign the long sequence to a reference genome. The H3.3 histones are shown in white, N-(1,10-phenanthroline-5-yl) iodoacetamide (Phe) is the label, it chelates a copper ion (Cu+) to DNA and the presence of hydrogen peroxide causes hydroxyl radical cleavage of DNA where copper is bound.

7. Nanopore sequencing of MNase-digested chromatin

In order to assess the feasibility of our strategy to map H3.3 containing telomeric nucleosomes, we performed sequencing of MNase-digested chromatin by Oxford Nanopore Technology (ONT). Several peculiar features distinguish ONT from most of the other next generation sequencing techniques. An ONT sequencing device consists of a polymer membrane in which are embedded hundreds-to-thousands of nanopores. A ionic current passes through the nanopore channels; when a DNA (or RNA) molecule is induced to go through the nanopore the current is altered in a sequence-dependent manner. Measuring the changes in current allows deducing the DNA sequence of each single molecule. Thus, ONT is a single-molecule sequencing technique, and PCR amplification is not necessary. A second feature is that sequencing efficiency and accuracy is independent from DNA length, allowing sequencing of DNA fragments several kb long. A third useful characteristic is that preparation of the library is easy and rapid and sequencing can be performed in your own lab, connecting the small MinION sequencer to a computer. There are also disadvantages: a higher error rate of basecalling and, since the methodology is quite new and not yet widespread, there is a limited availability of bioinformatic resources.

ONT has been used to study nucleosome spacing and organization in Drosophila (Baldi et al., 2018), whose genome is more than ten-fold smaller than human genome. This suggests the need for enriching in telomeric DNA to have a sufficient coverage of telomeric regions. In order to set-up a correct strategy we performed a pilot sequencing experiment. Chromatin from BJ cells was digested with MNase and the DNA extracted. Fig. 25 shows the typical pattern of MNase digested chromatin, with a ladder of nucleosomal repeats about 200-bp long. Before preparing the library, we bound MNase-digested DNA to AMPure beads at a v/v ratio of 0.6. This step allowed discarding most DNA smaller than

340 bp, that is most of the mononucleosomal and the dinucleosomal bands.

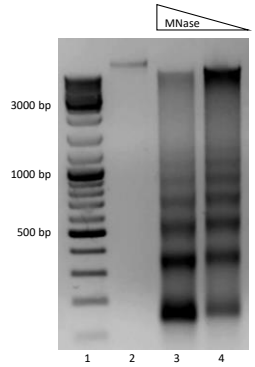

Fig. 25. Micrococcal digestion of BJhTERT genomic DNA. Two different concentration of the enzyme were used; respectively 222 (lane 3) and 74 (lane 4) units. As a control, genomic DNA was treated as the other samples without adding the enzyme (lane 2).

The purified DNA sample was end-repaired, A-tailed and ligated to ONT sequencing adapters. The resulting library has been sequenced on a MinION instrument using R9.4 flow cell, under control of the ONT MinKNOW software. Sequencing has been run for 36 h and generated 3,266,730 reads containing 2,421,206,552 bases. The raw data were basecalled by using the Guppy software. After quality filtering the sequence yield was of 2,830,124 reads containing 2,300,146,812 bases. The resulting library was searched for telomeric sequences, both by mapping reads to human genome and by directly scanning them for telomeric repeats (See Materials and Methods for details) . The reads filtered for having telomeric repeats are 1119 containing 725128 bases. The ratio between telomeric bases and the total sequenced bases is $3x10^{-4}$, in agreement with the fraction of telomeric DNA in the genome (about $1\text{-}3x10^{-4}$). The profile obtained reporting the number of reads and the length of all the sequenced fragments shows the typical MNase digestion profile (deprived of the mononucleosome and of the dinucleosome), with peaks every 180-200 bases (Fig. 26). Plotting only the reads with telomeric repeats shows instead a much shorter spacing of about 140-160 bases (Fig. 27), in agreement with previous analyses (Galati

et al., 2012; Makarov et al., 1993; Tommerup et al., 1994). Two populations are evident, indicated respectively in blue and red. Both populations have a 150-160 nucleosomal repeat. We hypothesized that one population derives from entirely telomeric reads, namely the blue peaks at 450 bp (trimer), 600 bp (tetramer), 750 bp (pentamer), 900 (examer). The second population might represent fragments spanning subtelomeric and telomeric repeats. The first peak of the red series, at 340, might be a dimer comprising the last subtelomeric nucleosome and the first telomeric nucleosome, connected by a 40-50 bp linker DNA. Then, the spacing is the typical telomeric short spacing, with peaks at 490 bp (trimer), 640 bp (tetramer), 780 bp (pentamer).

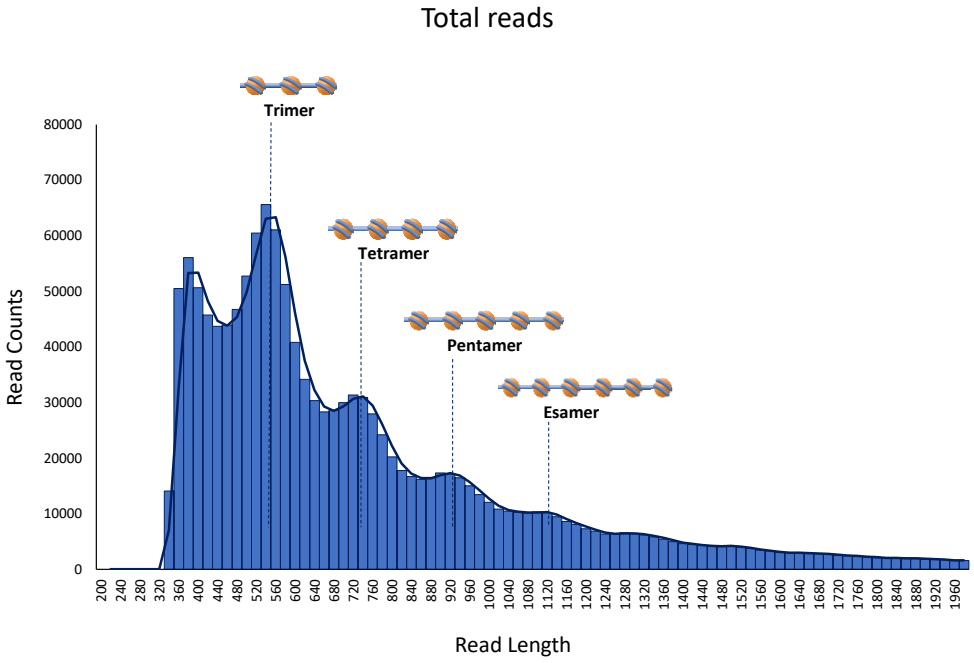

Fig. 26. Distribution of the 2,830,124 reads obtained from Nanopore sequencing of DNA fragments from a MNase digestion of BJ-hTERT chromatin. Reads have been plotted vs DNA length. Each bar reports reads spanning 20 bp. The trend shows the typical MNase digestion profile, with peaks every 180-200 bases.

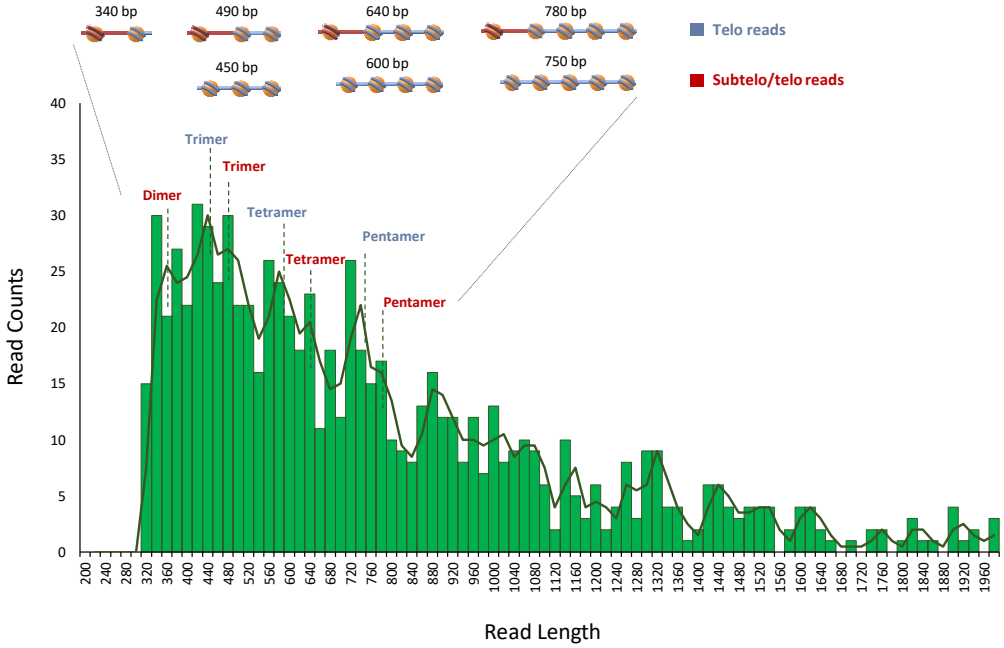

Fig. 27. Distribution of the 1119 reads containing telomeric repeats filtered from the library plotted in Fig. 26. Reads have been plotted vs DNA length. Each bar reports reads spanning 20 bp. The trend shows a MNase digestion profile with a shorter spacing (140-160 bases) (in blue) The second population showed in red might represent fragments spanning subtelomeric and telomeric repeats

Among the 1119 reads containing telomeric repeats, 302 were assigned to specific telomeres by aligning with the subtelomeric repeats. These results suggest that nanopore sequencing can potentially be used to map nucleosome positions at telomeres, but a much greater number of reads is needed. This can be obtained by a significant increase of the starting material. Then, an expensive option would be to perform several additional sequencing runs, otherwise, the starting material should be enriched in telomeric DNA.

8. Enrichment of telomeric DNA

In order to have an adequate sequencing coverage of telomeric DNA, we set up a protocol for telomeric enrichment. To simulate chemical or nuclease cleavage, the DNA was fragmented using EcoRI restriction enzyme. Since telomeric sequences have no recognition sites for restriction enzymes, this procedure leaves telomeres intact. 2 µg of digested genomic DNA was first blunt-end repaired and then A-tailed. Then, the resulting library was ligated to two previously phosphorylated adapters having a 3' protruding thymine (fig. 29). After being purified from unligated adapters by using AMPure XP magnetic beads, the samples were denatured and hybridized with blocking oligonucleotides complementary to the 5' and 3' ends, to avoid chaining between target (telomeric) and non-target DNA fragments due to non-specific binding of cross-reacting adapters. The samples were then dissolved in a specific hybridization buffer and incubated with a biotinylated $(TTACCC)_8$ probe to capture telomeric DNA. Upon hybridization, streptavidin magnetic beads were used to capture the biotinylated probes. After several washes at 65°C, the captured telomeres were eluted in 50 µL of Tris 5 mM.

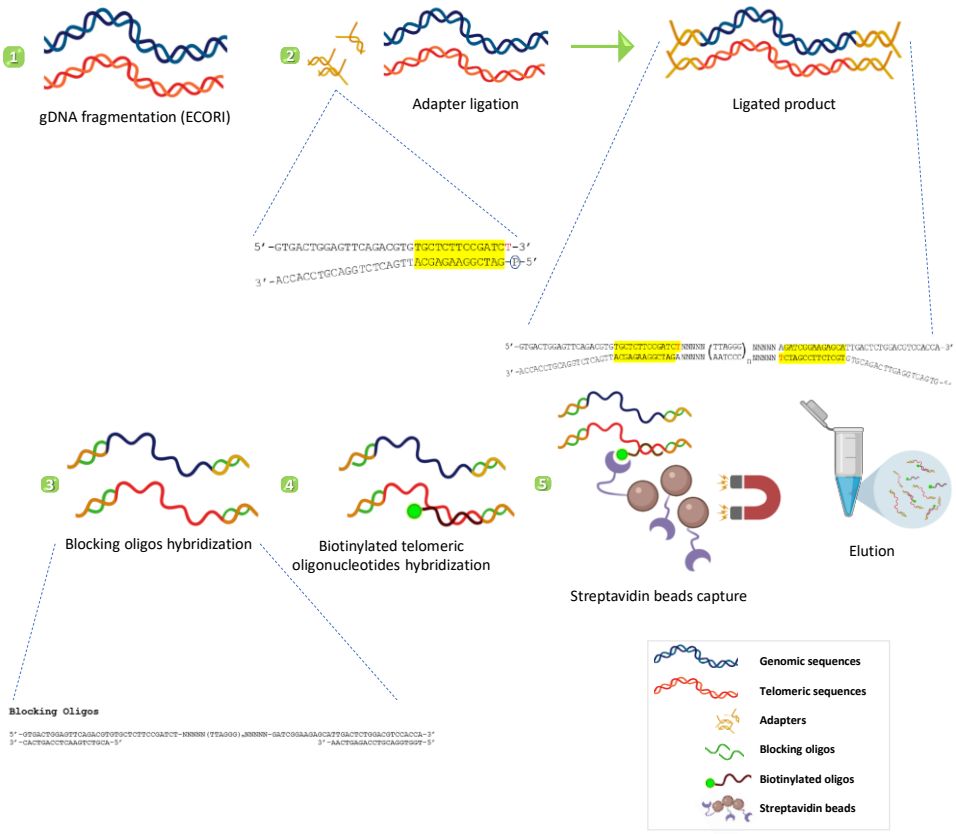

Fig. 29. Schematic representation of the telomeric enrichment workflow.

To evaluate the efficacy of the enrichment, we performed PCR amplification of subtelomeric and genomic regions (Fig. 30). A clear amplification product is evident by using primers from the subtelomeres of chromosomes Xp and Yp (SubXp/Yp) (Fig. 30, lane 12), whereas no PCR product is visible using primers from the *H3F3B* gene (Fig. 30, lanes 6 and 7). We checked also the presence of SubXp/Yp and H3F3B in the first wash after incubation with streptavidin dynabeads (Fig. 31). A band is evident also in the sample amplified with SubXp/Yp primers (Fig. 31, lane 5), even if less intense than in the control (Fig. 31, lane 4). This indicates that

part of the telomeric fraction has not been captured by the CCCTTA probe.

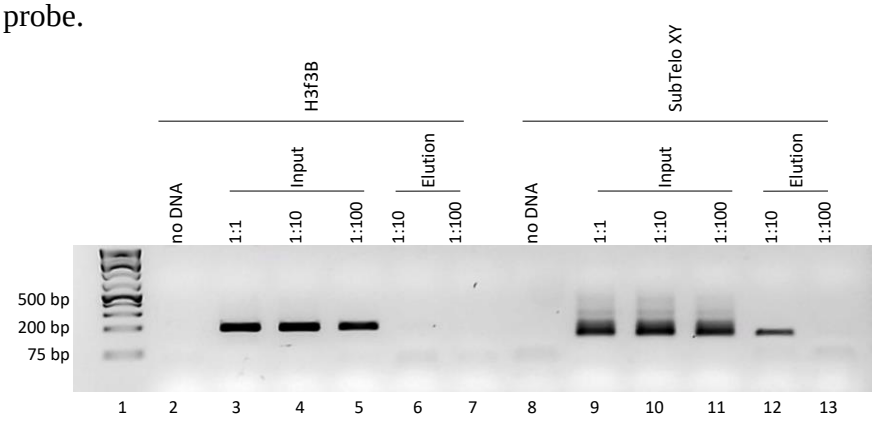

Fig. 30. PCR experiment on enriched telomeres. Lane 2 and 8: no DNA. 50 ng of the input DNA from BJ-hTERT fibroblasts digested and ligated to adapters was loaded at decreasing concentration: non diluted, 1:1 (lane 3 and 9), 1:10 dilution (lane 4 and 10) and 1:100 dilution (lane 5 and 11). The eluted sample enriched in telomeres was also employed at 2 different concentrations: 1:10 dilution (lane 6 and 12) and 1:100 dilution (lane 7 and 13). *H3F3B* fv and rv primers amplify 192 bp, SubTelo X/Y fv and rv primers amplify 180 bp.

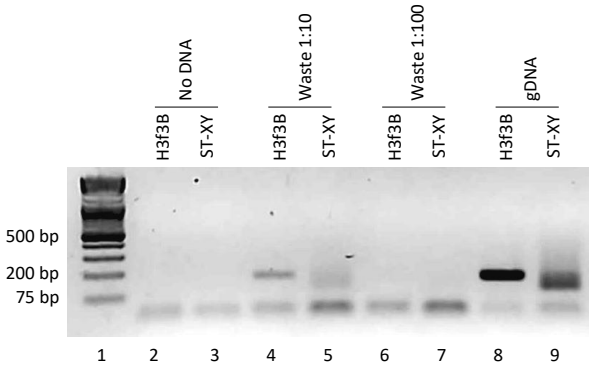

Fig. 31. Same PCR experiment as in fig. 30 using waste sample as template. Subtelomeric DNA is present also in the waste sample, even with a fainter signal than H3F3B, indicating that a part of telomeric DNA has not been sequestered by the biotinylated probe

To quantitively measure the extent of telomeric enrichment, we performed a real-time PCR (qPCR). Primers for the p-arm of the

subtelomere of chromosome 9 (st-9p) and for both the *H3F3A* and the *H3F3B* gene were utilized. Firstly, we constructed a standard curve for the three primers pairs (fig. 32). This was drawn using a 5-fold dilution series of known quantities of input DNA (40 – 8 – 1 – 0.32 – 0.064 ng). The logarithms of the copy numbers (roughly estimated as 2 copies per each 6 pg of DNA) are shown on the X axis, while the CT values are plotted on the Y axis.
St-9p, *H3F3A* (H33A) and *H3F3B* (H33A) copy numbers of input and enriched samples were extrapolated using the linear regression and reported in the histogram in fig. 33 as a percentage of the input. While genomic H33A and H33B were absent in the eluate, the recovery of telomeric DNA could be estimated around 20% (fig. 33). In the end, the enrichment protocol appeared to work properly and to collect a decent DNA quantity to proceed with the Nanopore-mediated sequencing.

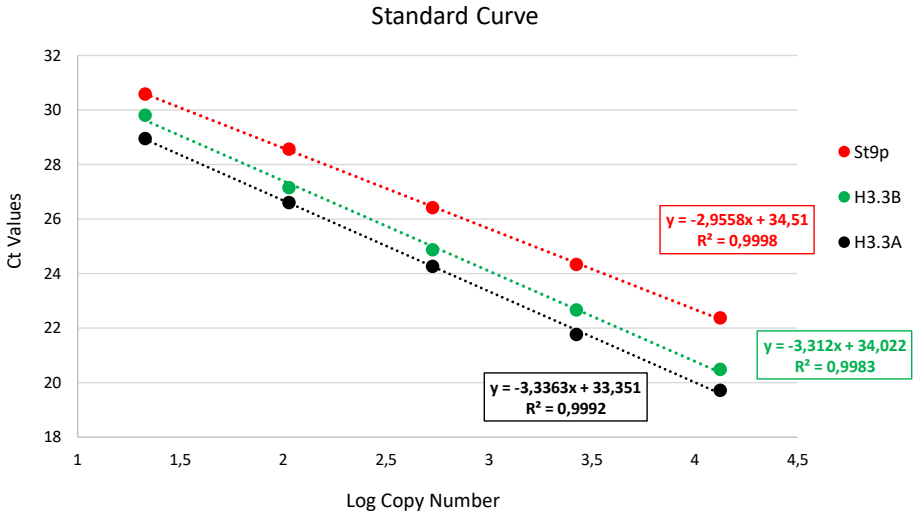

Fig. 32. Standard curves for *H3F3A* (H33A), *H3F3B* (H33B), subtelo 9p (st-9p).

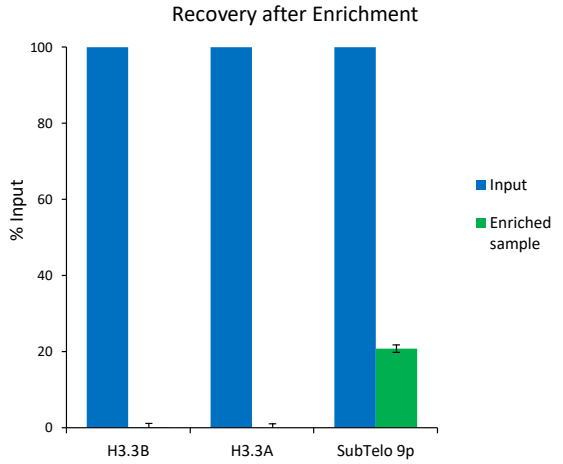

Fig. 33. Efficiency of enrichment recovery of telomeric DNA measured by Real-Time PCR of a subtelomeric sequence. Data are expressed as percent relative to input. All data are shown as the mean +/- SEM of three separate enrichment experiments.

A more accurate estimation of the enrichment yield comes from nanopore sequencing. We performed a sequencing run loading 200 ng of the control DNA (BJ genomic DNA digested with EcoRI) and the result of the enrichment starting from 2 µg of the same digested DNA sample. In the case of the control sample we obtained 555 telomeric reads out of 2237846 (1 telomeric read out of 4000 reads). Instead, in the case of the enriched sample there were 520 telomeric reads out of 4826 reads, that is one telomeric read out of 9 reads (Fig. 34).

	Input	telo/total reads	%
total reads	2237846	-	100%
telomeric reads	555	0,000248006	0,02%
1 telomeric read out of 4000 reads			

	enriched sample	telo/total reads	%
total reads	4826	-	100%
telomeric reads	520	0,107749689	11%
1 telomeric read out of 9 reads			

Fig. 34. Overview of the data obtained from the Nanopore sequencing on the control sample and after telomeric enrichment. The table lists the number of the total and telomeric reads and the percentage of telomeric reads.

DISCUSSION

Growing data are accumulating in support of a role for histone modifications, histone variants and chromatin remodeling factors (CRFs) in telomere maintenance (Benetti et al., 2007b; Galati et al., 2013; Palacios et al., 2010). In particular, SIRT6 is among the most extensively studied CRFs implicated in telomere integrity (Michishita et al., 2008). The role of SIRT6 in cancer is controversial. In some tumors, high levels of SIRT6 are associated with poorer outcomes (Huang et al., 2017; Khongkow et al., 2013). In other tumors, including colorectal cancer (CRC), SIRT6 seems to have tumor suppressive activity (Kugel et al., 2016; Marquardt et al., 2013; Liu et al., 2018). TRF2 was recently identified as a novel substrate of SIRT6, demonstrating that, upon DNA damage, SIRT6-dependent deacetylation of TRF2 promotes its degradation. An inverse correlation between SIRT6 and TRF2 protein expression levels have been also found in a cohort of CRC patients (Rizzo et al., 2017), suggesting that an impairment of TRF2 degradation, as a consequence of SIRT6 loss, could be one of the mechanisms underlying the increased dosages of TRF2 observed in many human malignancies. We investigated the mechanism/s by which SIRT6 regulates TRF2 binding to heterochromatin. First, we set up an *in vitro* model system previously used for the study of the TRF2 binding to linker DNA adjacent to nucleosomes (Galati et al., 2015). In particular, these binding assays were conducted also in the presence of purified SIRT6 to explore whether it affects TRF2 binding in a nucleosomal environment. We found that SIRT6, even in presence of a hypoacetylated nucleosome, has the capability of stabilizing the association of TRF2 to nucleosome *in vitro*. This feature might be relevant in telomeric chromatin homeostasis since TRF2 has a low affinity for nucleosomal binding sites (Galati et al., 2015). Support to SIRT6 role in TRF2 binding to chromatin comes from experiments of chromatin extractions in HCT-116 cells depleted of SIRT6. We found a significant decrease of TRF2 association with chromatin upon SIRT6 depletion, whereas the

association of SIRT6 with chromatin is not affected upon TRF2 depletion. To get more details on TRF2 decreased association upon SIRT6 depletion, we performed a ChIP experiment. From the dot-blot analyses using telomeric and SAT III probes it emerged that TRF2 levels decrease both at telomeres and pericentromeres.
By combining chromatin immunoprecipitation with high-throughput DNA sequencing (ChIP-seq), in control or SIRT6 silenced HCT116 cells, it emerged that SIRT6 depletion favors a switch of TRF2 binding from pericentromeric regions to gene expression related sequences, some of which implicated in cancer onset.
Collectively, these results indicate a functional role of SIRT6 in stabilizing TRF2 binding to heterochromatic regions. It seems reasonable to suppose that, in native conditions, SIRT6 has the capability of stabilizing the binding of TRF2 to chromatin whereas, upon DNA damage, it mediates its deacetylation and degradation (Rizzo et al., 2017). The delocalization of TRF2 from telomeres and pericentromeres, induced by SIRT6 loss in favor of the association with other regions of the genome may be explained by the fact that, once TRF2 loses the SIRT6 contribution for its stabilization on the chromatin, TRF2 can be instead stabilized in other sites by different factors. Furthermore, TRF2 localization on several gene promoters involved in cancer, raises the intriguing question whether SIRT6 downregulation observed in human tumors can be crucial in promoting the oncogenic properties of TRF2. Additionally, several papers show that increased dosages of TRF2 can influence tumor formation and progression through modulation of gene transcription (Biroccio et al., 2013; Zizza et al., 2019). The fact that TRF2 may directly affect gene expression implies that cancer cells expressing higher levels of TRF2 can activate a different transcriptional program compared to low TRF2 expressing cells. Therefore, further investigation will be necessary to assess the transcriptional effect of TRF2 on its putative target genes. Finally, additional studies are fundamental for a deeper comprehension of SIRT6-TRF2 association. The impact of SIRT6 depletion on histone

modifications and how this impact may affect the TRF2 binding it is not to be underestimated. It is known from literature that depletion of SIRT6 leads to cells dysfunctions and premature cell senescence, accompanied by increasing levels of acetylation on its targets, in particular at telomeres (Michishita et al., 2008; Yang et al., 2009) and at pericentromeres (Tasselli et al., 2016). This clearly could have an impact on the epigenetic state and on TRF2 affinity for chromatin, and further investigations are necessary to distinguish functions related to chromatin binding from those related to the enzymatic activity, for example by employing different SIRT6 catalytically inactive mutants (Hou et al., 2020).

Another poorly understood feature of telomeric chromatin is its enrichment in the histone variant H3.3.

H3.3 is expressed and incorporated into chromatin in a replication-independent way throughout the entire cell cycle; in particular, it is enriched in promoters and enhancers of actively transcribed genes and at pericentric and telomeric regions. H3.3 deposition is replication-independent and is mediated by different histone chaperones. HIRA complex mediates H3.3 deposition at active genes, whereas a different complex, ATRX/DAXX, is required for H3.3 deposition at telomeres and at pericentromeric regions (Szenker et al., 2011). The scientific interest for H3.3 has been recently highlighted by the discovery of recurrent H3.3 mutations in several pediatric brain cancers and bone tumors (Shi et al., 2017). At present, the role of the H3.3 histone variant is still matter of study; in particular, the reason why H3.3 is highly enriched at telomeres is far from being elucidated. Maps of H3.3 nucleosome positions along the human genome had been obtained by ChIP-seq. However, mapping H3.3 at telomeres is hampered by the particular features of telomeric sequences. The uniformly repeated sequence and the heterogeneous length of human telomeres impedes having any information on whether H3.3 nucleosomes are positioned at the very end of the chromosome or rather close to the subtelomeric region.

We addressed the issue of H3.3 role at telomeres developing an experimental strategy with two main objectives: i. Setting up a method to map H3.3 positions on the genome with base-pair accuracy. ii. Developing a procedure to obtain an oriented map of nucleosome positions at telomeres. To tackle the first task, we took advantage of the method developed by Henikoff and co-workers to map nucleosomes in yeast (Chereji et al., 2018). They mutated yeast H3 gene introducing a cysteine at 85 position (H3Q85C). The cysteine's sulfhydryl group binds covalently the agent Phenantroline added to the cells. Subsequent addition of copper and hydrogen peroxide catalyzes the formation of short-lived hydroxyl radicals that cleave the DNA backbone 20 bp from the dyad axis of the nucleosome. The 51 bp DNA fragments resulting by cleavage on either side of the dyad axis form a library of fragments allowing nucleosome position assignments at base pair accuracy (Chereji et al., 2018). We decided to apply this strategy to map H3.3 positions in human cells. The unique yeast H3 gene is H3.3-like. Moreover, H3.3 in humans is encoded by only two genes, while canonical histones H3.1 and H3.2 by 15 genes overall. We realized a transgene carrying the variant H3.3Q85C and tested the ability to express and localize on the chromatin. We generated transgenic human BJ fibroblasts and HeLa cells through lentivirus gene delivery and checked the expression of H3.3 Q85C and its localization into the nucleus. Then we proceeded with the setup of the chemical cleavage protocol. The validation of the chemical cleavage is a crucial point of this project, it has to be highly specific and the background degradation have to be reduced as much as possible. Indeed, the experimental evidences also described by (Brogaard et al., 2012; Voong et al., 2016) show a limited DNA degradation background caused by phenanthroline treatment. The chemical treatment has been tested on BJ-hTERT-H3.3Q85C fibroblast and HeLa-H3.3Q85C cells. The phenanthroline/copper/hydrogen peroxide treatment generated a robust degradation in H3.3Q85C cells, indicating an active chemical mediated DNA cleavage, whereas genomic DNA of BJ-hTERT and HeLa control cells is substantially

intact. This experiment is a clear proof of concept of the validity of this method in human cells.
The chemical cleavage generated a smear (DNA molecules of various dimension) but there is no trace of the 51 bp molecules deriving from double cleavage on the same nucleosome. The reason for this absence is that the transgene product H3.3Q85C represents only a fraction of total H3.3 and has to compete with the endogenous H3.3 for the incorporation within the nucleosome. As a consequence, it is unlikely that the mutant form of H3.3 is present twice on the same nucleosome. To map H3.3 position genome-wide, we are pursuing to mutate endogenous *H3F3A* and *H3F3B* genes by CRISPR-Cas knock-in.
Even if inadequate to map H3.3 positions genome-wide, the random and partial incorporation of H3.3Q85C within the chromatin can be exploited to define H3.3 nucleosome positions at telomeres. In the case of telomeres, analysis of the 51 bp DNA library that can be obtained by complete chemical digestion could give information on nucleosome occupancy, but not on nucleosome positions along the telomeres. Instead, a random partial cleavage would release fragments spanning also subtelomeric DNA, that could be used to determine the position of the cleavage on telomeric H3.3 nucleosomes. To this aim we planned to use a relatively new sequencing technique, that allow obtaining the sequence of very long DNA fragments, namely Oxford Nanopore sequencing. We realized two pilot experiments. First, we sequenced DNA from BJ cells digested with MNase to test the feasibility of nanopores to map telomeric nucleosome positions and spacing. We identified about one thousand telomeric reads. The analysis of the read lengths shows clearly that nucleosome spacing at telomeres is shorter than in the rest of chromatin. The number of reads obtained is however too small to allow nucleosome mapping of single telomeres. Since telomeric reads are only a small fraction of the total reads (1-3 out of 10000), we developed a protocol to enrich telomeric DNA, avoiding sequencing millions of undesired genomic sequences. We used biotinylated telomeric probes and streptavidin magnetic beads

to capture telomeric sequences. The enrichment was verified by real-time experiments and by a pilot sequencing experiment. The result was a very small number of reads but highly enriched in telomeric sequences, with one telomeric read out of nine total reads. In the near future we plan to combine chemical cleavage and telomere enrichment to obtain a more detailed map of H3.3 containing positions at telomeres. H3.3 plays a key role in gene regulation and in the maintenance of specific chromatin states. We have a still incomplete knowledge of H3.3 functions and many future studies are required to elucidate our lacks. Once set-up, we think that our mapping method could be a precious tool to get insights into H3.3 role and mechanism of action, and possibly open a new path in the study of ALT-positive cancers.

MATERIALS AND METHODS

Cells, culture condition and transfection

Cells were maintained in Dulbecco Modified eagle medium (D-MEM, Euroclone) containing 10% fetal bovine serum (FBS), 2mM L-glutamine and antibiotics. For transient RNA interference experiments, siCTR and siSIRT6 were purchased from Santa Cruz Biotechnology Inc. (Santa Cruz, CA, USA) and transfected into HCT116 with Interferin (Polyplus) according to the manufacturer's instructions.

Chromatin extraction

Cell membranes were lysed in 2-5 volumes of Lysis buffer (10 mM HEPES pH 7.4, 10 mM KCl, 0.05% NP-40, protease and phosphatase inhibitors). After centrifugation step (14,000 rpm at 4°C, 10 min), the supernatants containing cytoplasmatic protein extract were recovered. Then, pellets containing intact nuclei were washed once with lysis buffer and then centrifuged as before. After discarding the supernatants, nuclei were resuspended in Low-Salt buffer (10 mM Tris-HCl pH 7.4, 0.2 mM $MgCl_2$) and centrifuged at maximum speed for 10 mins at 4°C. Then, the pellets were treated with 2 volumes of 0.2 N HCl for acid extraction of the chromatin. Reaction was stopped with same volume of 1 M Tris-HCl pH 8. Samples were resolved with SDS-PAGE and processed for WB.

MNase digestion

$5x10^6$ cells were harvested and lysed in Buffer A (0.25 M sucrose, 10 mM Tris/HCl (pH 8.0), 10 mM $MgCl_2$, 1% v/v Triton X-100). Then, $CaCl_2$ was added to the samples, and chromatin was digested for 5 min with 222 and 74 Units of MNase enzyme (NEB). MNase reaction was stopped by adding one volume of TEES/proteinase K (10mM Tris HCl pH 7.5, 10mM EDTA, 10mM EGTA, 1% SDS, 50

g/ml proteinase K) and incubated at 37◦C overnight. DNA was phenol-extracted and run on a 1% agarose gel. For the sequencing with the Oxford Nanopore MinION, the samples were size selected with AMPure XP magnetic beads, in order to eliminates fragments smaller than about 300 bp.

Western blot

Cells were lysed in Lysis buffer (10 mM Tris-HCl pH 7.5, 150 mM NaCl, 0.5% Nonidet P-40, 0.5% sodium dodecyl sulfate (SDS), cocktail protease/phosphatase inhibitors, (Pierce)) and sonicated for a few seconds in ice. The concentration of proteins in the cellular extracts was determined with a BCA protein assay (Thermo Fisher Scientific). The protein lysate was resolved on SDS-PAGE and transferred onto the nitrocellulose filter. The filter was first incubated in a 5% milk powder TBS for 1 hour and then with the primary antibody overnight. Upon incubation with the secondary antibody, the protein bands were detected via chemiluminescence (ECL Western Blotting detection reagents, Amersham Life Science).

DNA fragments and nucleosome reconstitution

The Tel2-601-Tel2 DNA fragment was extracted from the plasmid by cutting with EcoRI and BamHI, labeled by filling in the ends with Klenow enzyme and [α-^{32}P] dATP, gel-purified (Galati et al., 2015). Nucleosome reconstitution was performed by mixing 1 picomole of labeled DNA with 1 µg nucleosome (chicken erythrocytes), in 1 M NaCl, 20 mM Hepes pH 7.9, 0.1% Nonidet-P40, 100 µg/ml bovine serum albumin (BSA), in a final volume of 10 µl. After incubation at room temperature for 30', the salt concentration was lowered to 0.1 MNaCl by sequential additions every 10' of 20 mM Hepes pH 7.9, 0.1% Nonidet-P40 (2, 4, 8, 16, 30, 30 µl).

Electrophoretic mobility-shift assay

Binding assays were performed by incubating proteins and reconstituted nucleosome in 15 µl of a reaction mix of 20 mM Hepes (pH 7.9), 100 mM NaCl, 50 mM KCl, 1 mM MgCl2, 0.1 mM ethylenediaminetetraacetic acid (EDTA), 1-mM DTT, 5% (v/v) glycerol, 0.5 mg/ml of BSA and 0.1% (v/v) NP-40. The reaction mix was incubated at 4◦C for 90 min and then run on native 4.5% polyacrylamide gels (37.5:1, 0.5 × TBE) or on a 0.8% (w/v) agarose gel (0.2 × TBE). Gel was dried and exposed to PhosphorImager screens and quantitated using ImageQuant (Amersham Biosciences).

ChIP and ChIP-seq

Cells were cross-linked with 1% formaldehyde. The reaction was stopped with glycine 0,125 M. Cellular membranes were disrupted with a dounce homogenizer. Nuclei were incubated in Hypotonic buffer (50 mM Tris, 10 mM KCl, 2 mM EDTA, 0.5% NP40, 0.1% DOC) and then resuspended and sonicated in Nucleus Lysis buffer (50 mM Tris, 10 mM EDTA, 1% SDS) until the average length of fragments reached 200 bp. The samples were diluted 10- folds to produce the final concentration of the ChIP buffer: : 50 mM Tris, 150 mM NaCl 2 mM EDTA, 1% Triton, and 0.1% SDS) The samples were incubated with the primary antibody overnight and then with protein G sepharose beads for 2 hours, washed with ChIP buffer, High-Salt buffer (50 mM Tris, 500 mM NaCl, 2 mM EDTA, 1% Triton, 0.1% SDS) and with LiCl buffer (50 mM Tris, 250 mM LiCl, 2 mM EDTA, 0.5% NP40, 0.5% DOC). Chromatin was released with solution 1%SDS in 0.1M NaHCO3 at 65° for 15 minutes. The crosslink was reversed by incubating the samples in Tris (final concentration 20 mM), NaCl (200 mM), EDTA (2 mM), RNase A (100 µg/ml) at 65°C overnight. Then, DNA was treated with proteinase K for 1 h at 45° and then extracted with phenol-chloroform purification. The samples from ChIP was denatured (0.5

M NaOH, 2 M NaCl and 25 mM EDTA) and blotted onto nylon membranes using a dot blot apparatus, crosslinked, and hybridized with telomeric, pericentromeric and Alu probes, radioactively labeled. The membranes were exposed onto Phosphor-imager screens and the signal intensity was quantified with ImageQuant software. The differential peaks positions found for the TRF2 ChIP-Seq were identified during the annotation step of the ChIP-Seq analysis by using the Homer tools suite. The bioinformatic analysis was realized thanks to the support of the Eric Gilson's laboratory (IRCAN, Faculty of Medicine Nice, France; Department of Genetics).

Chemical cleavage

Trypsinized cells were pelleted and resuspended in Permeabilization buffer (150 mM sucrose, 80 mM KCl, 35 mM HEPES pH 7.4, 5 mM K2HPO4, 5 mM MgCl2) and L-a-lysophosphatidylcholine at a final concentration of 100 mg/mL for 5 min. Permeabilized and again pelleted cells were then washed in Wash buffer (150 Mm Sucrose, 10mM Tris-HCl pH 7.4, 15 mM NaCl, 60 Mm KCl, 5 mM MgCl2, 0.01% NP-40, 0.5 mM spermidine, 0.15 mM spermine), and incubated with 1.4 mM N-(1,10- Phenanthrolin-5-yl) iodoacetamide (Biotium) for 2 hours at RT. Washes with Mapping buffer (150 mM Sucrose, 50 mM Tris-HCl pH 7.5, 2.5 mM NaCl, 60 mM KCl, 5 mM MgCl2, 0.01% NP-40, 0.5 mM spermidine (Sigma), 0.15 mM spermine) followed and the pelleted cells were incubated with 0.15 mM CuCl2 for 2 minutes. They were later washed, resuspended in mapping buffer and exposed for 20 minutes to hydroxyl radical cleavage using 6 mM of 3-mercaptopropanoic acid (Alfa-Aesar) and 6 mM of H2O2. The mapping reaction was quenched with 2.8 mM Neocuproine (Alfa Aesar) and, lastly, to extract the chemically cleaved DNA, the cell pellets were lysed in a buffer containing 10 mM Tris-HCl pH 8.0, 25 mM EDTA, 100 mM NaCl, 0.5% SDS, and 0.2 mg/mL proteinase K overnight at 55°C. Following phenol/chloroform extraction, ethanol precipitation, and RNase A

treatment at 20 mg/mL, the purified DNA was resolved on a 2% Agarose gel.

Cloning

Mutant H3.3AQ85C cDNA was purchased by Genewiz and digested with EcoRI and BamHI at 37°C overnight. The gene sequences were gel-purified with the 'Isolate II PCR & Gel' kit (Bio-Line), ligated in pCDH-3XFLAG-puro and finally transformed in competent bacteria overnight at 37°C. Plasmids from selected colonies screened via PCR were extracted with the 'HiPure plasmid midi prep' kit (Invitrogen).

Infections

Human BJ-hTERT and HeLa cell lines were infected with lentiviral vectors to deliver *H3F3A*Q85C. HCT-116 was infected with pLKO.1-shTRF2 plasmid. The viruses were assembled into HEK293T, transfected with PMD 2.6, R874 the pCDH or pLKO plasmids. The culture medium was substituted 24 hours after the transfection, while the lentivirus-containing medium was harvested at 2 and 3 days from the transfection. $1{,}5x10^5$ Human BJ-hTERT, HeLa cells and HCT-116 were seeded 1-day prior the infection. 1 day after the infection, the selection antibiotic (Puromycin) was added with fresh culture medium at a final concentration of 5 μg/ml.

Immunofluorescence

$5x10^4$ cells were fixed with 2% formaldehyde and permeabilized in 0.25% Triton X100 in phosphate buffered saline (PBS) for 5 minutes at RT. Fixed and permeabilized cells were first incubated with the primary and then with the secondary antibodies. To tracking the nucleus, cells were counterstained with DAPI. Fluorescence signals were analysed with a Leica DMIRE2 Microscope, equipped with a

Leica DFC 350FX camera and elaborated by Leica FW4000 deconvolution software (Leica).

Antibodies

List of antibodies used for the WB: polyclonal antibody (pAb) anti-FLAG (Sigma), pAb anti-SIRT6 (Novus), pAb anti-H3 (Abcam) and mAb anti-β-actin (Sigma) as a normalizer. List of antibodies employed for the IF: pAb anti-FLAG (Sigma), anti-rabbit FITC (Alexa Fluor), mAb anti-TRF2 (Millipore) and anti-mouse TRITC (Alexa Fluor). Antibodies used for ChIP and ChIP-seq: pAb anti-TRF2 (Novus); pAb anti-H3K18Ac (Millipore), pAb IgG (Santa Cruz Biotechnology).

Purification of His-tag proteins

6xHis-tagged SIRT6 plasmid was kindly gifted from John Denu (Addgene plasmid #13739). The vector was transformed in TOP 10 E. coli, grown until OD 600 0,6. The induction was performed by added of 0.1 mM IPTG for 4 h at 25°C. 6xHis-tagged TRF2 was transformed and expressed in BL21(D3) and grown until OD 600 0,6. The induction was made by added of 1 mM IPTG for 4 h at 37°C. Cells were lysed by sonication and resuspended with Ni-resin for 1 h. Then, the resin was washed and protein eluted according to the manufacturer's instructions. The proteins was dialyzed using Slide-A-Lyzer Dialysis cassette (Thermo scientific Pierce,Waltham,MA, USA) in 50 mM Tris pH 7.5, 150 mM NaCl, 10% glycerol (wt/vol), and 5 mM DTT and stored at −20◦C before use.

Genomic DNA purification

Cells were lysed in Lysis buffer, RNase A and Proteinase K. Upon phenol-chloroform extraction (x2), DNA was precipitated at -20°C with 3M sodium acetate and 2 volumes of pure ethanol. The samples

were centrifuged, and the supernatants were carefully discarded. The pellets were washed twice in 70% ethanol and let dry. Then, DNA were resuspended in Elution buffer.

Telomeric enrichment

The first step requires adapters preparation. Two adapters (fig. 26) were designed to repair the digested DNA ends (Ad1_3' and Ad1_5', or Ad2_3' and Ad2_5'). After the phosphorylation of the reverse oligonucleotide with T4 PNK for 20 minutes at 37°C, Ad1_3' and 5' were hybridized in an oligo hybridization buffer 10X (500 mM NaCl, 10 mM Tris-Cl pH 8.0, 1 mM EDTA pH 8.0) in a final volume of 50 µL and at a final concentration of 40 µM. The Adapters mix was then incubated in a thermal cycler for 2 min at 95°C, followed by a ramp-down to 12°C at a rate of 0,1°C/sec.).
The second step includes DNA preparation and adapters ligation. 2 µg of EcoRI-digested gDNA was repaired and A-tailed with NEBNext Multiplex Oligos (New England Bio-Labs) and subsequently ligated to 2.5 µL of adapters mix using the NEB next ultra II Ligation master. The mixture was then incubated at 20°C for 15 minutes. 0.4:1 µL AMPure XP magnetic beads (Beckman culture Life Science) were employed to isolate long DNA fragments and discard oligo contaminants.
The third step hybridizes the obtained DNA library with biotinylated probes. Blocking oligos (BO1_3' and BO1_5') were added to the adapter-ligated library at a final concentration of 2 µL, in order to block the DNA extremities and avoid the formation of non-specific aggregations. Blocking oligo-adapter-ligated library was later dried completely in a SpeedVac set at 45°C. A hybridization buffer 2X from xGen Lockdown Reagents kit (Integrated DNA technologies) was added to the dried sample and after a denaturation step at 95°C for 10 minutes, biotinylated probes BIO-$(TTACCC)_8$ were immediately added to the reaction mixture at a final concentration of 0,5 µM. To compare hybridization efficiencies, this hybridization

step was performed in double: one line at 65°C and another at 42°C. The samples were incubated overnight in a thermal cycler.
The fourth step allows telomeric DNA capture. 100 µL of Dynabeads MyOne Streptavidin C1 (Invitrogen) were used for each capture. After several rounds of washes required for beads equilibration, the hybridized targets were bound to streptavidin beads with a thermocycler step at 65°C for 45 minutes. After two different washes, one at 65°C and one at RT, with wash buffers provided with the xGen Lockdown Reagents kit (Integrated DNA technologies), the magnetic beads with captured DNA were eluted in 50 µL of Tris 5 mM following the standard Dynabeads protocol.

Real Time PCR

The enriched DNA samples and the initial digested gDNA used for the enrichment were used as a template. The subtelomere of chr. 9 p-arm (Subtelo 9p fw + rv), *H3F3A* (H3.3A 222 fw + rv) and *H3F3B* gene (H3.3B 192 fw + rv) were the targets. SYBR Green was used as intercalating fluorescent agent (SensiFAST SYBR, Bio-Line) and the amplification reaction was performed with Quantum Studio 3 PCR System (Applied Biosystems) running the following program: 3 minutes at 95°C, 5 seconds at 95°C and 30 seconds at 62°C, for 40 cycles. The results were analysed with QuantStudio Design and Analysis Software.

Sequencing with Oxford Nanopore technology

For the sequencing process we chose the MinION platform of Oxford Nanopore technology. Data acquisition, real-time analysis and platform check were all performed with the Oxford Nanopore MinKNOW software. High-accuracy basecalling was performed using Guppy software. Flow cell type: FLO-MIN 106, kit: SQK-LSK 109, MinKNOW Core version: 3.6.5, Bream: 4.3.16, Guppy: 3.2.10. Reads shorter than 100 nucleotides and those with low Phred quality score were removed using Filtlong tool, available at

https://github.com/rrwick/Filtlong. Reads containing telomeric repeats were identified using different tools: edgeCase (https://www.biorxiv.org/content/10.1101/2020.01.31.929307v1) to search for tags mapping to the ends of chromosomes and extending past them into telomeric regions, nhmmer (https://academic.oup.com/bioinformatics/article/29/19/2487/186765) and LAST (https://academic.oup.com/bioinformatics/article/33/6/926/2585025) to directly search for telomeric repeats within read sequences. The bioinformatic analysis was realized thanks to the support of Gian Gaetano Tartaglia, Alessio Colantoni and Gabriele Proietti (Dept. of Biology and Biotechnology, Sapienza University)

REFERENCES

Abreu, E., Aritonovska, E., Reichenbach, P., Cristofari, G., Culp, B., Terns, R.M., Lingner, J., and Terns, M.P. (2010). TIN2-tethered TPP1 recruits human telomerase to telomeres in vivo. Mol Cell Biol *30*, 2971-2982.

Augereau, A., T'Kint de Roodenbeke, C., Simonet, T., Bauwens, S., Horard, B., Callanan, M., Leroux, D., Jallades, L., Salles, G., Gilson, E., *et al.* (2011). Telomeric damage in early stage of chronic lymphocytic leukemia correlates with shelterin dysregulation. Blood *118*, 1316-1322.

Avogaro, L., Querido, E., Dalachi, M., Jantsch, M.F., Chartrand, P., and Cusanelli, E. (2018). Live-cell imaging reveals the dynamics and function of single-telomere TERRA molecules in cancer cells. RNA Biol *15*, 787-796.

Azzalin, C.M., Reichenbach, P., Khoriauli, L., Giulotto, E., and Lingner, J. (2007). Telomeric repeat containing RNA and RNA surveillance factors at mammalian chromosome ends. Science *318*, 798-801.

Bae, N.S., and Baumann, P. (2007). A RAP1/TRF2 complex inhibits nonhomologous end-joining at human telomeric DNA ends. Mol Cell *26*, 323-334.

Baker, A.M., Fu, Q., Hayward, W., Lindsay, S.M., and Fletcher, T.M. (2009). The Myb/SANT domain of the telomere-binding protein TRF2 alters chromatin structure. Nucleic Acids Res *37*, 5019-5031.

Baldi, S., Krebs, S., Blum, H., and Becker, P.B. (2018). Genome-wide measurement of local nucleosome array regularity and spacing by nanopore sequencing. Nat Struct Mol Biol *25*, 894-901.

Barral, A., and Dejardin, J. (2020). Telomeric Chromatin and TERRA. J Mol Biol *432*, 4244-4256.

Baumann, P., and Cech, T.R. (2001). Pot1, the putative telomere end-binding protein in fission yeast and humans. Science *292*, 1171-1175.

Behjati, S., Tarpey, P.S., Presneau, N., Scheipl, S., Pillay, N., Van Loo, P., Wedge, D.C., Cooke, S.L., Gundem, G., Davies, H., *et al.* (2013). Distinct H3F3A and H3F3B driver mutations define chondroblastoma and giant cell tumor of bone. Nat Genet *45*, 1479-1482.

Bender, S., Tang, Y., Lindroth, A.M., Hovestadt, V., Jones, D.T., Kool, M., Zapatka, M., Northcott, P.A., Sturm, D., Wang, W., *et al.* (2013). Reduced H3K27me3 and DNA hypomethylation are major drivers of gene expression in K27M mutant pediatric high-grade gliomas. Cancer Cell *24*, 660-672.

Benetti, R., Garcia-Cao, M., and Blasco, M.A. (2007a). Telomere length regulates the epigenetic status of mammalian telomeres and subtelomeres. Nat Genet *39*, 243-250.

Benetti, R., Gonzalo, S., Jaco, I., Schotta, G., Klatt, P., Jenuwein, T., and Blasco, M.A. (2007b). Suv4-20h deficiency results in telomere elongation and derepression of telomere recombination. J Cell Biol *178*, 925-936.

Berardinelli, F., Sgura, A., Facoetti, A., Leone, S., Vischioni, B., Ciocca, M., and Antoccia, A. (2018). The G-quadruplex-stabilizing ligand RHPS4 enhances sensitivity of U251MG glioblastoma cells to clinical carbon ion beams. FEBS J *285*, 1226-1236.

Berardinelli, F., Siteni, S., Tanzarella, C., Stevens, M.F., Sgura, A., and Antoccia, A. (2015). The G-quadruplex-stabilising agent RHPS4 induces telomeric dysfunction and enhances radiosensitivity in glioblastoma cells. DNA Repair (Amst) *25*, 104-115.

Biroccio, A., Cherfils-Vicini, J., Augereau, A., Pinte, S., Bauwens, S., Ye, J., Simonet, T., Horard, B., Jamet, K., Cervera, L., *et al.* (2013). TRF2 inhibits a cell-extrinsic pathway through which natural killer cells eliminate cancer cells. Nat Cell Biol *15*, 818-828.

Blackburn, E.H. (1991). Structure and function of telomeres. Nature *350*, 569-573.

Blackburn, E.H. (1992). Telomerases. Annu Rev Biochem *61*, 113-129.

Bradshaw, P.S., Stavropoulos, D.J., and Meyn, M.S. (2005). Human telomeric protein TRF2 associates with genomic double-strand breaks as an early response to DNA damage. Nat Genet *37*, 193-197.
Brogaard, K.R., Xi, L., Wang, J.P., and Widom, J. (2012). A chemical approach to mapping nucleosomes at base pair resolution in yeast. Methods Enzymol *513*, 315-334.
Bryan, T.M., Englezou, A., Gupta, J., Bacchetti, S., and Reddel, R.R. (1995). Telomere elongation in immortal human cells without detectable telomerase activity. EMBO J *14*, 4240-4248.
Burge, S., Parkinson, G.N., Hazel, P., Todd, A.K., and Neidle, S. (2006). Quadruplex DNA: sequence, topology and structure. Nucleic Acids Res *34*, 5402-5415.
Cacchione, S., Biroccio, A., and Rizzo, A. (2019). Emerging roles of telomeric chromatin alterations in cancer. J Exp Clin Cancer Res *38*, 21.
Cacchione, S., Cerone, M.A., and Savino, M. (1997). In vitro low propensity to form nucleosomes of four telomeric sequences. FEBS Lett *400*, 37-41.
Celli, G.B., and de Lange, T. (2005). DNA processing is not required for ATM-mediated telomere damage response after TRF2 deletion. Nat Cell Biol *7*, 712-718.
Cesare, A.J., and Griffith, J.D. (2004). Telomeric DNA in ALT cells is characterized by free telomeric circles and heterogeneous t-loops. Mol Cell Biol *24*, 9948-9957.
Cesare, A.J., and Reddel, R.R. (2010). Alternative lengthening of telomeres: models, mechanisms and implications. Nat Rev Genet *11*, 319-330.
Chang, F.T., Chan, F.L., JD, R.M., Udugama, M., Mayne, L., Collas, P., Mann, J.R., and Wong, L.H. (2015). CHK1-driven histone H3.3 serine 31 phosphorylation is important for chromatin maintenance and cell survival in human ALT cancer cells. Nucleic Acids Res *43*, 2603-2614.
Chartrand, P., and Sfeir, A. (2020). A single-molecule view of telomerase regulation at telomeres. Mol Cell Oncol *7*, 1818537.

Chereji, R.V., Ramachandran, S., Bryson, T.D., and Henikoff, S. (2018). Precise genome-wide mapping of single nucleosomes and linkers in vivo. Genome Biol *19*, 19.
Cherfils-Vicini, J., Iltis, C., Cervera, L., Pisano, S., Croce, O., Sadouni, N., Gyorffy, B., Collet, R., Renault, V.M., Rey-Millet, M., *et al.* (2019). Cancer cells induce immune escape via glycocalyx changes controlled by the telomeric protein TRF2. EMBO J *38*.
Clynes, D., Jelinska, C., Xella, B., Ayyub, H., Scott, C., Mitson, M., Taylor, S., Higgs, D.R., and Gibbons, R.J. (2015). Suppression of the alternative lengthening of telomere pathway by the chromatin remodelling factor ATRX. Nat Commun *6*, 7538.
Cristofari, G., and Lingner, J. (2006). Telomere length homeostasis requires that telomerase levels are limiting. EMBO J *25*, 565-574.
Cubiles, M.D., Barroso, S., Vaquero-Sedas, M.I., Enguix, A., Aguilera, A., and Vega-Palas, M.A. (2018). Epigenetic features of human telomeres. Nucleic Acids Res *46*, 2347-2355.
Cusanelli, E., Romero, C.A., and Chartrand, P. (2013). Telomeric noncoding RNA TERRA is induced by telomere shortening to nucleate telomerase molecules at short telomeres. Mol Cell *51*, 780-791.
de Lange, T. (2005). Shelterin: the protein complex that shapes and safeguards human telomeres. Genes Dev *19*, 2100-2110.
de Lange, T. (2018). Shelterin-Mediated Telomere Protection. Annu Rev Genet.
De Vitis, M., Berardinelli, F., and Sgura, A. (2018). Telomere Length Maintenance in Cancer: At the Crossroad between Telomerase and Alternative Lengthening of Telomeres (ALT). Int J Mol Sci *19*.
Denchi, E.L., and de Lange, T. (2007). Protection of telomeres through independent control of ATM and ATR by TRF2 and POT1. Nature *448*, 1068-1071.
Deng, Z., Norseen, J., Wiedmer, A., Riethman, H., and Lieberman, P.M. (2009). TERRA RNA binding to TRF2 facilitates heterochromatin formation and ORC recruitment at telomeres. Mol Cell *35*, 403-413.

Diala, I., Wagner, N., Magdinier, F., Shkreli, M., Sirakov, M., Bauwens, S., Schluth-Bolard, C., Simonet, T., Renault, V.M., Ye, J., *et al.* (2013). Telomere protection and TRF2 expression are enhanced by the canonical Wnt signalling pathway. EMBO Rep *14*, 356-363.

Dilley, R.L., and Greenberg, R.A. (2015). ALTernative Telomere Maintenance and Cancer. Trends Cancer *1*, 145-156.

Doksani, Y., and de Lange, T. (2016). Telomere-Internal Double-Strand Breaks Are Repaired by Homologous Recombination and PARP1/Lig3-Dependent End-Joining. Cell Reports *17*, 1646-1656.

El Mai, M., Wagner, K.D., Michiels, J.F., Ambrosetti, D., Borderie, A., Destree, S., Renault, V., Djerbi, N., Giraud-Panis, M.J., Gilson, E., *et al.* (2014). The Telomeric Protein TRF2 Regulates Angiogenesis by Binding and Activating the PDGFRbeta Promoter. Cell Rep *9*, 1047-1060.

Elsaesser, S.J., Goldberg, A.D., and Allis, C.D. (2010). New functions for an old variant: no substitute for histone H3.3. Curr Opin Genet Dev *20*, 110-117.

Episkopou, H., Draskovic, I., Van Beneden, A., Tilman, G., Mattiussi, M., Gobin, M., Arnoult, N., Londono-Vallejo, A., and Decottignies, A. (2014). Alternative Lengthening of Telomeres is characterized by reduced compaction of telomeric chromatin. Nucleic Acids Res *42*, 4391-4405.

Ernst, J., Kheradpour, P., Mikkelsen, T.S., Shoresh, N., Ward, L.D., Epstein, C.B., Zhang, X., Wang, L., Issner, R., Coyne, M., *et al.* (2011). Mapping and analysis of chromatin state dynamics in nine human cell types. Nature *473*, 43-49.

Fang, D., Gan, H., Lee, J.H., Han, J., Wang, Z., Riester, S.M., Jin, L., Chen, J., Zhou, H., Wang, J., *et al.* (2016). The histone H3.3K36M mutation reprograms the epigenome of chondroblastomas. Science *352*, 1344-1348.

Fang, J., Huang, Y., Mao, G., Yang, S., Rennert, G., Gu, L., Li, H., and Li, G.M. (2018). Cancer-driving H3G34V/R/D mutations block H3K36 methylation and H3K36me3-MutSalpha interaction. Proc Natl Acad Sci U S A *115*, 9598-9603.

Feng, J., Funk, W.D., Wang, S.S., Weinrich, S.L., Avilion, A.A., Chiu, C.P., Adams, R.R., Chang, E., Allsopp, R.C., Yu, J., *et al.* (1995). The RNA component of human telomerase. Science *269*, 1236-1241.

Feretzaki, M., Renck Nunes, P., and Lingner, J. (2019). Expression and differential regulation of human TERRA at several chromosome ends. RNA *25*, 1470-1480.

Filesi, I., Cacchione, S., De Santis, P., Rossetti, L., and Savino, M. (2000). The main role of the sequence-dependent DNA elasticity in determining the free energy of nucleosome formation on telomeric DNAs. Biophys Chem *83*, 223-237.

Filipescu, D., Szenker, E., and Almouzni, G. (2013). Developmental roles of histone H3 variants and their chaperones. Trends Genet *29*, 630-640.

Fontebasso, A.M., Papillon-Cavanagh, S., Schwartzentruber, J., Nikbakht, H., Gerges, N., Fiset, P.O., Bechet, D., Faury, D., De Jay, N., Ramkissoon, L.A., *et al.* (2014). Recurrent somatic mutations in ACVR1 in pediatric midline high-grade astrocytoma. Nat Genet *46*, 462-466.

Fouche, N., Cesare, A.J., Willcox, S., Ozgur, S., Compton, S.A., and Griffith, J.D. (2006). The basic domain of TRF2 directs binding to DNA junctions irrespective of the presence of TTAGGG repeats. J Biol Chem *281*, 37486-37495.

Frank, D., Doenecke, D., and Albig, W. (2003). Differential expression of human replacement and cell cycle dependent H3 histone genes. Gene *312*, 135-143.

Galati, A., Magdinier, F., Colasanti, V., Bauwens, S., Pinte, S., Ricordy, R., Giraud-Panis, M.J., Pusch, M.C., Savino, M., Cacchione, S., *et al.* (2012). TRF2 controls telomeric nucleosome organization in a cell cycle phase-dependent manner. PLoS One *7*, e34386.

Galati, A., Micheli, E., Alicata, C., Ingegnere, T., Cicconi, A., Pusch, M.C., Giraud-Panis, M.J., Gilson, E., and Cacchione, S. (2015). TRF1 and TRF2 binding to telomeres is modulated by nucleosomal organization. Nucleic Acids Res *43*, 5824-5837.

Galati, A., Micheli, E., and Cacchione, S. (2013). Chromatin structure in telomere dynamics. Front Oncol *3*, 46.
Galati, A., Rossetti, L., Pisano, S., Chapman, L., Rhodes, D., Savino, M., and Cacchione, S. (2006). The human telomeric protein TRF1 specifically recognizes nucleosomal binding sites and alters nucleosome structure. J Mol Biol *360*, 377-385.
Garcia-Cao, M., O'Sullivan, R., Peters, A.H., Jenuwein, T., and Blasco, M.A. (2004). Epigenetic regulation of telomere length in mammalian cells by the Suv39h1 and Suv39h2 histone methyltransferases. Nat Genet *36*, 94-99.
Gilson, E., and Geli, V. (2007). How telomeres are replicated. Nat Rev Mol Cell Biol *8*, 825-838.
Gilson, E., and Londono-Vallejo, A. (2007). Telomere length profiles in humans: all ends are not equal. Cell Cycle *6*, 2486-2494.
Giraud-Panis, M.J., Pisano, S., Poulet, A., Le Du, M.H., and Gilson, E. (2010). Structural identity of telomeric complexes. FEBS Lett *584*, 3785-3799.
Goldberg, A.D., Banaszynski, L.A., Noh, K.M., Lewis, P.W., Elsaesser, S.J., Stadler, S., Dewell, S., Law, M., Guo, X., Li, X., *et al.* (2010). Distinct factors control histone variant H3.3 localization at specific genomic regions. Cell *140*, 678-691.
Gong, Y., and de Lange, T. (2010). A Shld1-controlled POT1a provides support for repression of ATR signaling at telomeres through RPA exclusion. Mol Cell *40*, 377-387.
Graf, M., Bonetti, D., Lockhart, A., Serhal, K., Kellner, V., Maicher, A., Jolivet, P., Teixeira, M.T., and Luke, B. (2017). Telomere Length Determines TERRA and R-Loop Regulation through the Cell Cycle. Cell *170*, 72-85 e14.
Harkness, R.W.t., and Mittermaier, A.K. (2017). G-quadruplex dynamics. Biochim Biophys Acta Proteins Proteom *1865*, 1544-1554.
Heaphy, C.M., de Wilde, R.F., Jiao, Y., Klein, A.P., Edil, B.H., Shi, C., Bettegowda, C., Rodriguez, F.J., Eberhart, C.G., Hebbar, S., *et al.* (2011). Altered telomeres in tumors with ATRX and DAXX mutations. Science *333*, 425.

Henson, J.D., Hannay, J.A., McCarthy, S.W., Royds, J.A., Yeager, T.R., Robinson, R.A., Wharton, S.B., Jellinek, D.A., Arbuckle, S.M., Yoo, J., *et al.* (2005). A robust assay for alternative lengthening of telomeres in tumors shows the significance of alternative lengthening of telomeres in sarcomas and astrocytomas. Clin Cancer Res *11*, 217-225.

Herbig, U., Jobling, W.A., Chen, B.P., Chen, D.J., and Sedivy, J.M. (2004). Telomere shortening triggers senescence of human cells through a pathway involving ATM, p53, and p21(CIP1), but not p16(INK4a). Mol Cell *14*, 501-513.

Hou, T., Cao, Z., Zhang, J., Tang, M., Tian, Y., Li, Y., Lu, X., Chen, Y., Wang, H., Wei, F.Z., *et al.* (2020). SIRT6 coordinates with CHD4 to promote chromatin relaxation and DNA repair. Nucleic Acids Res *48*, 2982-3000.

Huang, N., Liu, Z.W., Zhu, J.B., Cui, Z.Q., Li, Y.G., Yu, Y.C., Sun, F.Y., Pan, Q.H., and Yang, Q.Y. (2017). Sirtuin 6 plays an oncogenic role and induces cell autophagy in esophageal cancer cells. Tumor Biology *39*, 1-13.

Huppert, J.L., and Balasubramanian, S. (2005). Prevalence of quadruplexes in the human genome. Nucleic Acids Res *33*, 2908-2916.

Hussain, T., Saha, D., Purohit, G., Kar, A., Mukherjee, A.K., Sharma, S., Sengupta, S., Dhapola, P., Maji, B., Vedagopuram, S., *et al.* (2017). Transcription regulation of CDKN1A (p21/CIP1/WAF1) by TRF2 is epigenetically controlled through the REST repressor complex. Scientific Reports *7*.

Izumi, H., and Funa, K. (2019). Telomere Function and the G-Quadruplex Formation are Regulated by hnRNP U. Cells *8*.

Jia, G., Su, L., Singhal, S., and Liu, X. (2012). Emerging roles of SIRT6 on telomere maintenance, DNA repair, metabolism and mammalian aging. Mol Cell Biochem *364*, 345-350.

Jiao, L., and Liu, X. (2015). Structural basis of histone H3K27 trimethylation by an active polycomb repressive complex 2. Science *350*, aac4383.

Karlseder, J., Broccoli, D., Dai, Y., Hardy, S., and de Lange, T. (1999). p53- and ATM-dependent apoptosis induced by telomeres lacking TRF2. Science *283*, 1321-1325.
Khongkow, M., Olmos, Y., Gong, C., Gomes, A.R., Monteiro, L.J., Yague, E., Cavaco, T.B., Khongkow, P., Man, E.P.S., Laohasinnarong, S., *et al.* (2013). SIRT6 modulates paclitaxel and epirubicin resistance and survival in breast cancer. Carcinogenesis *34*, 1476-1486.
Kim, N.W., Piatyszek, M.A., Prowse, K.R., Harley, C.B., West, M.D., Ho, P.L., Coviello, G.M., Wright, W.E., Weinrich, S.L., and Shay, J.W. (1994). Specific association of human telomerase activity with immortal cells and cancer. Science *266*, 2011-2015.
Kugel, S., and Mostoslavsky, R. (2014). Chromatin and beyond: the multitasking roles for SIRT6. Trends Biochem Sci *39*, 72-81.
Kugel, S., Sebastian, C., Fitamant, J., Ross, K.N., Saha, S.K., Jain, E., Gladden, A., Arora, K.S., Kato, Y., Rivera, M.N., *et al.* (2016). SIRT6 Suppresses Pancreatic Cancer through Control of Lin28b. Cell *165*, 1401-1415.
Kwon, J.H., Shin, J.H., Kim, E.S., Lee, N., Park, J.Y., Koo, B.S., Hong, S.M., Park, C.W., and Choi, K.Y. (2012). REST-dependent expression of TRF2 renders non-neuronal cancer cells resistant to DNA damage during oxidative stress. Int J Cancer.
Lei, M., Podell, E.R., and Cech, T.R. (2004). Structure of human POT1 bound to telomeric single-stranded DNA provides a model for chromosome end-protection. Nat Struct Mol Biol *11*, 1223-1229.
Lim, J., Park, J.H., Baude, A., Yoo, Y., Lee, Y.K., Schmidt, C.R., Park, J.B., Fellenberg, J., Zustin, J., Haller, F., *et al.* (2017). The histone variant H3.3 G34W substitution in giant cell tumor of the bone link chromatin and RNA processing. Sci Rep *7*, 13459.
Lin, T.T., Letsolo, B.T., Jones, R.E., Rowson, J., Pratt, G., Hewamana, S., Fegan, C., Pepper, C., and Baird, D.M. (2010). Telomere dysfunction and fusion during the progression of chronic lymphocytic leukemia: evidence for a telomere crisis. Blood *116*, 1899-1907.

Liu, D., O'Connor, M.S., Qin, J., and Songyang, Z. (2004). Telosome, a mammalian telomere-associated complex formed by multiple telomeric proteins. J Biol Chem *279*, 51338-51342.
Liu, J.Q., Chen, C.Y., Xue, Y., Hao, Y.H., and Tan, Z. (2010). G-quadruplex hinders translocation of BLM helicase on DNA: a real-time fluorescence spectroscopic unwinding study and comparison with duplex substrates. J Am Chem Soc *132*, 10521-10527.
Liu, W.G., Wu, M.W., Du, H.C., Shi, X.L., Zhang, T., and Li, J. (2018). SIRT6 inhibits colorectal cancer stem cell proliferation by targeting CDC25A. Oncology Letters *15*, 5368-5374.
Liu, W.H., Zheng, J., Feldman, J.L., Klein, M.A., Kuznetsov, V.I., Peterson, C.L., Griffin, P.R., and Denu, J.M. (2020). Multivalent interactions drive nucleosome binding and efficient chromatin deacetylation by SIRT6. Nat Commun *11*, 5244.
Londono-Vallejo, J.A., Der-Sarkissian, H., Cazes, L., Bacchetti, S., and Reddel, R.R. (2004). Alternative lengthening of telomeres is characterized by high rates of telomeric exchange. Cancer Res *64*, 2324-2327.
Lopez de Silanes, I., Grana, O., De Bonis, M.L., Dominguez, O., Pisano, D.G., and Blasco, M.A. (2014). Identification of TERRA locus unveils a telomere protection role through association to nearly all chromosomes. Nat Commun *5*, 4723.
Lovejoy, C.A., Li, W., Reisenweber, S., Thongthip, S., Bruno, J., de Lange, T., De, S., Petrini, J.H., Sung, P.A., Jasin, M., *et al.* (2012). Loss of ATRX, Genome Instability, and an Altered DNA Damage Response Are Hallmarks of the Alternative Lengthening of Telomeres Pathway. PLoS Genet *8*, e1002772.
Lowary, P.T., and Widom, J. (1998). New DNA sequence rules for high affinity binding to histone octamer and sequence-directed nucleosome positioning. J Mol Biol *276*, 19-42.
Maciejowski, J., and de Lange, T. (2017). Telomeres in cancer: tumour suppression and genome instability. Nat Rev Mol Cell Biol *18*, 175-186.
Mackay, A., Burford, A., Carvalho, D., Izquierdo, E., Fazal-Salom, J., Taylor, K.R., Bjerke, L., Clarke, M., Vinci, M., Nandhabalan, M.,

et al. (2017). Integrated Molecular Meta-Analysis of 1,000 Pediatric High-Grade and Diffuse Intrinsic Pontine Glioma. Cancer Cell *32*, 520-537 e525.
Makarov, V.L., Hirose, Y., and Langmore, J.P. (1997). Long G tails at both ends of human chromosomes suggest a C strand degradation mechanism for telomere shortening. Cell *88*, 657-666.
Makarov, V.L., Lejnine, S., Bedoyan, J., and Langmore, J.P. (1993). Nucleosomal organization of telomere-specific chromatin in rat. Cell *73*, 775-787.
Mao, Z., Hine, C., Tian, X., Van Meter, M., Au, M., Vaidya, A., Seluanov, A., and Gorbunova, V. (2011). SIRT6 promotes DNA repair under stress by activating PARP1. Science *332*, 1443-1446.
Marion, R.M., Schotta, G., Ortega, S., and Blasco, M.A. (2011). Suv4-20h abrogation enhances telomere elongation during reprogramming and confers a higher tumorigenic potential to iPS cells. PLoS One *6*, e25680.
Marquardt, J.U., Fischer, K., Baus, K., Kashyap, A., Ma, S.Y., Krupp, M., Linke, M., Teufel, A., Zechner, U., Strand, D., *et al.* (2013). Sirtuin-6-Dependent Genetic and Epigenetic Alterations Are Associated With Poor Clinical Outcome in Hepatocellular Carcinoma Patients. Hepatology *58*, 1054-1064.
Martadinata, H., Heddi, B., Lim, K.W., and Phan, A.T. (2011). Structure of long human telomeric RNA (TERRA): G-quadruplexes formed by four and eight UUAGGG repeats are stable building blocks. Biochemistry *50*, 6455-6461.
Mason, M., Schuller, A., and Skordalakes, E. (2011). Telomerase structure function. Curr Opin Struct Biol *21*, 92-100.
Mattern, K.A., Swiggers, S.J., Nigg, A.L., Lowenberg, B., Houtsmuller, A.B., and Zijlmans, J.M. (2004). Dynamics of protein binding to telomeres in living cells: implications for telomere structure and function. Mol Cell Biol *24*, 5587-5594.
McKittrick, E., Gafken, P.R., Ahmad, K., and Henikoff, S. (2004). Histone H3.3 is enriched in covalent modifications associated with active chromatin. Proc Natl Acad Sci U S A *101*, 1525-1530.

Mei, Z., Zhang, X., Yi, J., Huang, J., He, J., and Tao, Y. (2016). Sirtuins in metabolism, DNA repair and cancer. J Exp Clin Cancer Res *35*, 182.
Mendez-Bermudez, A., Lototska, L., Bauwens, S., Giraud-Panis, M.J., Croce, O., Jamet, K., Irizar, A., Mowinckel, M., Koundrioukoff, S., Nottet, N., *et al.* (2018). Genome-wide Control of Heterochromatin Replication by the Telomere Capping Protein TRF2. Mol Cell *70*, 449-461 e445.
Michishita, E., McCord, R.A., Berber, E., Kioi, M., Padilla-Nash, H., Damian, M., Cheung, P., Kusumoto, R., Kawahara, T.L., Barrett, J.C., *et al.* (2008). SIRT6 is a histone H3 lysine 9 deacetylase that modulates telomeric chromatin. Nature *452*, 492-496.
Michishita, E., McCord, R.A., Boxer, L.D., Barber, M.F., Hong, T., Gozani, O., and Chua, K.F. (2009). Cell cycle-dependent deacetylation of telomeric histone H3 lysine K56 by human SIRT6. Cell Cycle *8*, 2664-2666.
Mohammad, F., and Helin, K. (2017). Oncohistones: drivers of pediatric cancers. Genes & development *31*, 2313-2324.
Montero, J.J., Lopez de Silanes, I., Grana, O., and Blasco, M.A. (2016). Telomeric RNAs are essential to maintain telomeres. Nat Commun *7*, 12534.
Moyzis, R.K., Buckingham, J.M., Cram, L.S., Dani, M., Deaven, L.L., Jones, M.D., Meyne, J., Ratliff, R.L., and Wu, J.R. (1988). A highly conserved repetitive DNA sequence, (TTAGGG)n, present at the telomeres of human chromosomes. Proc Natl Acad Sci U S A *85*, 6622-6626.
Mukherjee, A.K., Sharma, S., Bagri, S., Kutum, R., Kumar, P., Hussain, A., Singh, P., Saha, D., Kar, A., Dash, D., *et al.* (2019). Telomere repeat-binding factor 2 binds extensively to extra-telomeric G-quadruplexes and regulates the epigenetic status of several gene promoters. J Biol Chem *294*, 17709-17722.
Munoz, P., Blanco, R., Flores, J.M., and Blasco, M.A. (2005). XPF nuclease-dependent telomere loss and increased DNA damage in mice overexpressing TRF2 result in premature aging and cancer. Nat Genet *37*, 1063-1071.

Nacev, B.A., Feng, L., Bagert, J.D., Lemiesz, A.E., Gao, J., Soshnev, A.A., Kundra, R., Schultz, N., Muir, T.W., and Allis, C.D. (2019). The expanding landscape of 'oncohistone' mutations in human cancers. Nature *567*, 473-478.

Nakanishi, K., Kawai, T., Kumaki, F., Hiroi, S., Mukai, M., Ikeda, E., Koering, C.E., and Gilson, E. (2003). Expression of mRNAs for telomeric repeat binding factor (TRF)-1 and TRF2 in atypical adenomatous hyperplasia and adenocarcinoma of the lung. Clin Cancer Res *9*, 1105-1111.

Nergadze, S.G., Farnung, B.O., Wischnewski, H., Khoriauli, L., Vitelli, V., Chawla, R., Giulotto, E., and Azzalin, C.M. (2009). CpG-island promoters drive transcription of human telomeres. RNA *15*, 2186-2194.

Nguyen, D.T., Voon, H.P.J., Xella, B., Scott, C., Clynes, D., Babbs, C., Ayyub, H., Kerry, J., Sharpe, J.A., Sloane-Stanley, J.A., *et al.* (2017). The chromatin remodelling factor ATRX suppresses R-loops in transcribed telomeric repeats. EMBO Rep *18*, 914-928.

Niehrs, C., and Luke, B. (2020). Regulatory R-loops as facilitators of gene expression and genome stability. Nat Rev Mol Cell Biol.

O'Sullivan, R.J., Kubicek, S., Schreiber, S.L., and Karlseder, J. (2010). Reduced histone biosynthesis and chromatin changes arising from a damage signal at telomeres. Nat Struct Mol Biol *17*, 1218-1225.

Oganesian, L., and Karlseder, J. (2013). 5' C-rich telomeric overhangs are an outcome of rapid telomere truncation events. DNA Repair (Amst) *12*, 238-245.

Olovnikov, A.M. (1973). A theory of marginotomy. The incomplete copying of template margin in enzymic synthesis of polynucleotides and biological significance of the phenomenon. J Theor Biol *41*, 181-190.

Palacios, J.A., Herranz, D., De Bonis, M.L., Velasco, S., Serrano, M., and Blasco, M.A. (2010). SIRT1 contributes to telomere maintenance and augments global homologous recombination. J Cell Biol *191*, 1299-1313.

Palm, W., and de Lange, T. (2008). How shelterin protects mammalian telomeres. Annu Rev Genet *42*, 301-334.
Pathania, M., De Jay, N., Maestro, N., Harutyunyan, A.S., Nitarska, J., Pahlavan, P., Henderson, S., Mikael, L.G., Richard-Londt, A., Zhang, Y., *et al.* (2017). H3.3(K27M) Cooperates with Trp53 Loss and PDGFRA Gain in Mouse Embryonic Neural Progenitor Cells to Induce Invasive High-Grade Gliomas. Cancer Cell *32*, 684-700 e689.
Perera, O.N., Sobinoff, A.P., Teber, E.T., Harman, A., Maritz, M.F., Yang, S.F., Pickett, H.A., Cesare, A.J., Arthur, J.W., MacKenzie, K.L., *et al.* (2019). Telomerase promotes formation of a telomere protective complex in cancer cells. Sci Adv *5*, eaav4409.
Petti, E., Buemi, V., Zappone, A., Schillaci, O., Broccia, P.V., Dinami, R., Matteoni, S., Benetti, R., and Schoeftner, S. (2019). SFPQ and NONO suppress RNA:DNA-hybrid-related telomere instability. Nat Commun *10*, 1001.
Phair, R.D., Scaffidi, P., Elbi, C., Vecerova, J., Dey, A., Ozato, K., Brown, D.T., Hager, G., Bustin, M., and Misteli, T. (2004). Global nature of dynamic protein-chromatin interactions in vivo: three-dimensional genome scanning and dynamic interaction networks of chromatin proteins. Mol Cell Biol *24*, 6393-6402.
Pickett, H.A., and Reddel, R.R. (2015). Molecular mechanisms of activity and derepression of alternative lengthening of telomeres. Nat Struct Mol Biol *22*, 875-880.
Pisano, S., and Gilson, E. (2019). Analysis of DNA-Protein Complexes by Atomic Force Microscopy Imaging: The Case of TRF2-Telomeric DNA Wrapping. Methods Mol Biol *1886*, 75-97.
Pisano, S., Leoni, D., Galati, A., Rhodes, D., Savino, M., and Cacchione, S. (2010). The human telomeric protein hTRF1 induces telomere-specific nucleosome mobility. Nucleic Acids Res *38*, 2247-2255.
Pisano, S., Marchioni, E., Galati, A., Mechelli, R., Savino, M., and Cacchione, S. (2007). Telomeric nucleosomes are intrinsically mobile. J Mol Biol *369*, 1153-1162.

Poncet, D., Belleville, A., t'kint de Roodenbeke, C., Roborel de Climens, A., Ben Simon, E., Merle-Beral, H., Callet-Bauchu, E., Salles, G., Sabatier, L., Delic, J., *et al.* (2008). Changes in the expression of telomere maintenance genes suggest global telomere dysfunction in B-chronic lymphocytic leukemia. Blood *111*, 2388-2391.

Porro, A., Feuerhahn, S., Delafontaine, J., Riethman, H., Rougemont, J., and Lingner, J. (2014). Functional characterization of the TERRA transcriptome at damaged telomeres. Nat Commun *5*, 5379.

Porro, A., Feuerhahn, S., Reichenbach, P., and Lingner, J. (2010). Molecular dissection of telomeric repeat-containing RNA biogenesis unveils the presence of distinct and multiple regulatory pathways. Mol Cell Biol *30*, 4808-4817.

Poulet, A., Buisson, R., Faivre-Moskalenko, C., Koelblen, M., Amiard, S., Montel, F., Cuesta-Lopez, S., Bornet, O., Guerlesquin, F., Godet, T., *et al.* (2009). TRF2 promotes, remodels and protects telomeric Holliday junctions. EMBO J *28*, 641-651.

Rezazadeh, S., Yang, D., Biashad, S.A., Firsanov, D., Takasugi, M., Gilbert, M., Tombline, G., Bhanu, N.V., Garcia, B.A., Seluanov, A., *et al.* (2020). SIRT6 mono-ADP ribosylates KDM2A to locally increase H3K36me2 at DNA damage sites to inhibit transcription and promote repair. Aging (Albany NY) *12*, 11165-11184.

Rezazadeh, S., Yang, D., Tombline, G., Simon, M., Regan, S.P., Seluanov, A., and Gorbunova, V. (2019). SIRT6 promotes transcription of a subset of NRF2 targets by mono-ADP-ribosylating BAF170. Nucleic Acids Res *47*, 7914-7928.

Rhodes, D., and Lipps, H.J. (2015). G-quadruplexes and their regulatory roles in biology. Nucleic Acids Res *43*, 8627-8637.

Rippe, K., and Luke, B. (2015). TERRA and the state of the telomere. Nat Struct Mol Biol *22*, 853-858.

Rizzo, A., Iachettini, S., Salvati, E., Zizza, P., Maresca, C., D'Angelo, C., Benarroch-Popivker, D., Capolupo, A., Del Gaudio, F., Cosconati, S., *et al.* (2017). SIRT6 interacts with TRF2 and

promotes its degradation in response to DNA damage. Nucleic Acids Res *45*, 1820-1834.
Rosenfeld, J.A., Wang, Z., Schones, D.E., Zhao, K., DeSalle, R., and Zhang, M.Q. (2009). Determination of enriched histone modifications in non-genic portions of the human genome. BMC Genomics *10*, 143.
Rossetti, L., Cacchione, S., Fua, M., and Savino, M. (1998). Nucleosome assembly on telomeric sequences. Biochemistry *37*, 6727-6737.
Salvati, E., Leonetti, C., Rizzo, A., Scarsella, M., Mottolese, M., Galati, R., Sperduti, I., Stevens, M.F., D'Incalci, M., Blasco, M., *et al.* (2007). Telomere damage induced by the G-quadruplex ligand RHPS4 has an antitumor effect. J Clin Invest *117*, 3236-3247.
Schmidt, J.C., Zaug, A.J., and Cech, T.R. (2016). Live Cell Imaging Reveals the Dynamics of Telomerase Recruitment to Telomeres. Cell *166*, 1188-1197 e1189.
Schoeftner, S., and Blasco, M.A. (2008). Developmentally regulated transcription of mammalian telomeres by DNA-dependent RNA polymerase II. Nat Cell Biol *10*, 228-236.
Schoeftner, S., and Blasco, M.A. (2010). Chromatin regulation and non-coding RNAs at mammalian telomeres. Semin Cell Dev Biol *21*, 186-193.
Schwartzentruber, J., Korshunov, A., Liu, X.Y., Jones, D.T., Pfaff, E., Jacob, K., Sturm, D., Fontebasso, A.M., Quang, D.A., Tonjes, M., *et al.* (2012). Driver mutations in histone H3.3 and chromatin remodelling genes in paediatric glioblastoma. Nature *482*, 226-231.
Sfeir, A., Kosiyatrakul, S.T., Hockemeyer, D., MacRae, S.L., Karlseder, J., Schildkraut, C.L., and de Lange, T. (2009). Mammalian telomeres resemble fragile sites and require TRF1 for efficient replication. Cell *138*, 90-103.
Shay, J.W. (2016). Role of Telomeres and Telomerase in Aging and Cancer. Cancer Discovery *6*, 584-593.
Shay, J.W., and Bacchetti, S. (1997). A survey of telomerase activity in human cancer. Eur J Cancer *33*, 787-791.

Shi, L., Wen, H., and Shi, X. (2017). The Histone Variant H3.3 in Transcriptional Regulation and Human Disease. J Mol Biol *429*, 1934-1945.
Simonet, T., Zaragosi, L.E., Philippe, C., Lebrigand, K., Schouteden, C., Augereau, A., Bauwens, S., Ye, J., Santagostino, M., Giulotto, E., *et al.* (2011). The human TTAGGG repeat factors 1 and 2 bind to a subset of interstitial telomeric sequences and satellite repeats. Cell Res *21*, 1028-1038.
Soman, A., Liew, C.W., Teo, H.L., Berezhnoy, N.V., Olieric, V., Korolev, N., Rhodes, D., and Nordenskiold, L. (2020). The human telomeric nucleosome displays distinct structural and dynamic properties. Nucleic Acids Res *48*, 5383-5396.
Spirkoski, J., Shah, A., Reiner, A.H., Collas, P., and Delbarre, E. (2019). PML modulates H3.3 targeting to telomeric and centromeric repeats in mouse fibroblasts. Biochem Biophys Res Commun *511*, 882-888.
Szenker, E., Ray-Gallet, D., and Almouzni, G. (2011). The double face of the histone variant H3.3. Cell Res *21*, 421-434.
Takai, K.K., Hooper, S., Blackwood, S., Gandhi, R., and de Lange, T. (2010). In vivo stoichiometry of shelterin components. J Biol Chem *285*, 1457-1467.
Tan, J., Duan, M., Yadav, T., Phoon, L., Wang, X., Zhang, J.M., Zou, L., and Lan, L. (2020). An R-loop-initiated CSB-RAD52-POLD3 pathway suppresses ROS-induced telomeric DNA breaks. Nucleic Acids Res *48*, 1285-1300.
Tan, J., and Lan, L. (2020). The DNA secondary structures at telomeres and genome instability. Cell Biosci *10*, 47.
Tasselli, L., Xi, Y., Zheng, W., Tennen, R.I., Odrowaz, Z., Simeoni, F., Li, W., and Chua, K.F. (2016). SIRT6 deacetylates H3K18ac at pericentric chromatin to prevent mitotic errors and cellular senescence. Nat Struct Mol Biol *23*, 434-440.
Tennen, R.I., Bua, D.J., Wright, W.E., and Chua, K.F. (2011). SIRT6 is required for maintenance of telomere position effect in human cells. Nat Commun *2*, 433.

Tommerup, H., Dousmanis, A., and de Lange, T. (1994). Unusual chromatin in human telomeres. Mol Cell Biol *14*, 5777-5785.
Udugama, M., FT, M.C., Chan, F.L., Tang, M.C., Pickett, H.A., JD, R.M., Mayne, L., Collas, P., Mann, J.R., and Wong, L.H. (2015). Histone variant H3.3 provides the heterochromatic H3 lysine 9 tri-methylation mark at telomeres. Nucleic Acids Res *43*, 10227-10237.
Uringa, E.J., Lisaingo, K., Pickett, H.A., Brind'amour, J., Rohde, J.H., Zelensky, A., Essers, J., and Lansdorp, P.M. (2012). RTEL1 contributes to DNA replication, repair and telomere maintenance. Mol Biol Cell.
van Steensel, B., and de Lange, T. (1997). Control of telomere length by the human telomeric protein TRF1. Nature *385*, 740-743.
Vannier, J.B., Pavicic-Kaltenbrunner, V., Petalcorin, M.I., Ding, H., and Boulton, S.J. (2012). RTEL1 dismantles T loops and counteracts telomeric G4-DNA to maintain telomere integrity. Cell *149*, 795-806.
Venneti, S., Garimella, M.T., Sullivan, L.M., Martinez, D., Huse, J.T., Heguy, A., Santi, M., Thompson, C.B., and Judkins, A.R. (2013). Evaluation of histone 3 lysine 27 trimethylation (H3K27me3) and enhancer of Zest 2 (EZH2) in pediatric glial and glioneuronal tumors shows decreased H3K27me3 in H3F3A K27M mutant glioblastomas. Brain Pathol *23*, 558-564.
von Zglinicki, T., Saretzki, G., Ladhoff, J., d'Adda di Fagagna, F., and Jackson, S.P. (2005). Human cell senescence as a DNA damage response. Mechanisms of ageing and development *126*, 111-117.
Voong, L.N., Xi, L., Sebeson, A.C., Xiong, B., Wang, J.P., and Wang, X. (2016). Insights into Nucleosome Organization in Mouse Embryonic Stem Cells through Chemical Mapping. Cell *167*, 1555-1570 e1515.
Wang, W.W., Zeng, Y., Wu, B., Deiters, A., and Liu, W.R. (2016). A Chemical Biology Approach to Reveal Sirt6-targeted Histone H3 Sites in Nucleosomes. ACS Chem Biol *11*, 1973-1981.
Wong, L.H., McGhie, J.D., Sim, M., Anderson, M.A., Ahn, S., Hannan, R.D., George, A.J., Morgan, K.A., Mann, J.R., and Choo, K.H. (2010). ATRX interacts with H3.3 in maintaining telomere

structural integrity in pluripotent embryonic stem cells. Genome Res *20*, 351-360.
Wong, L.H., Ren, H., Williams, E., McGhie, J., Ahn, S., Sim, M., Tam, A., Earle, E., Anderson, M.A., Mann, J., *et al.* (2009). Histone H3.3 incorporation provides a unique and functionally essential telomeric chromatin in embryonic stem cells. Genome research *19*, 404-414.
Wu, P., and de Lange, T. (2008). No overt nucleosome eviction at deprotected telomeres. Mol Cell Biol *28*, 5724-5735.
Wu, P., Takai, H., and de Lange, T. (2012). Telomeric 3' Overhangs Derive from Resection by Exo1 and Apollo and Fill-In by POT1b-Associated CST. Cell *150*, 39-52.
Wu, R.A., Dagdas, Y.S., Yilmaz, S.T., Yildiz, A., and Collins, K. (2015). Single-molecule imaging of telomerase reverse transcriptase in human telomerase holoenzyme and minimal RNP complexes. Elife *4*.
Xin, H., Liu, D., and Songyang, Z. (2008). The telosome/shelterin complex and its functions. Genome Biol *9*, 232.
Xu, Y., Kaminaga, K., and Komiyama, M. (2008). G-quadruplex formation by human telomeric repeats-containing RNA in Na+ solution. J Am Chem Soc *130*, 11179-11184.
Yang, B., Zwaans, B.M., Eckersdorff, M., and Lombard, D.B. (2009). The sirtuin SIRT6 deacetylates H3 K56Ac in vivo to promote genomic stability. Cell Cycle *8*, 2662-2663.
Yang, S., Zheng, X., Lu, C., Li, G.M., Allis, C.D., and Li, H. (2016). Molecular basis for oncohistone H3 recognition by SETD2 methyltransferase. Genes Dev *30*, 1611-1616.
Yeager, T.R., Neumann, A.A., Englezou, A., Huschtscha, L.I., Noble, J.R., and Reddel, R.R. (1999). Telomerase-negative immortalized human cells contain a novel type of promyelocytic leukemia (PML) body. Cancer Res *59*, 4175-4179.
Zahler, A.M., Williamson, J.R., Cech, T.R., and Prescott, D.M. (1991). Inhibition of telomerase by G-quartet DNA structures. Nature *350*, 718-720.

Zhang, M., Liu, R., and Wang, F. (2019). Telomere and G-Quadruplex Colocalization Analysis by Immunofluorescence Fluorescence In Situ Hybridization (IF-FISH). Methods Mol Biol *1999*, 327-333.
Zhang, Y., Shan, C.M., Wang, J., Bao, K., Tong, L., and Jia, S. (2017). Molecular basis for the role of oncogenic histone mutations in modulating H3K36 methylation. Sci Rep *7*, 43906.
Zimmer, J., Tacconi, E.M.C., Folio, C., Badie, S., Porru, M., Klare, K., Tumiati, M., Markkanen, E., Halder, S., Ryan, A., *et al.* (2016). Targeting BRCA1 and BRCA2 Deficiencies with G-Quadruplex-Interacting Compounds. Mol Cell *61*, 449-460.
Zizza, P., Dinami, R., Porru, M., Cingolani, C., Salvati, E., Rizzo, A., D'Angelo, C., Petti, E., Amoreo, C.A., Mottolese, M., *et al.* (2019). TRF2 positively regulates SULF2 expression increasing VEGF-A release and activity in tumor microenvironment. Nucleic Acids Res *47*, 3365-3382.

LIST OF PUBLICATIONS

Publications:

Pompili L, Maresca C, **Dello Stritto A**, Biroccio A, Salvati E. BRCA2 Deletion Induces Alternative Lengthening of Telomeres in Telomerase Positive Colon Cancer Cells. Genes (Basel). 2019 Sep 10;10(9):697.

Presentations:

Dello Stritto A, Maresca C, Pompili L, D'Angelo C, Graziani G, Biroccio A, Salvati E. TRF1 PARylation by PARP1 is required for the accomplishment of telomere replication.

At 2018 SIBBM Congress in Rome, Italy 20-22 June 2018.
At 2018 FISV Congress in Rome, Italy 18-21 September 2018.

RINGRAZIAMENTI

A conclusione di questo lavoro di tesi, è doveroso porre i miei più sentiti ringraziamenti alle persone che mi hanno aiutata a crescere sia dal punto di vista professionale che umano e senza le quali questo elaborato non sarebbe stato portato a termine nel miglior modo possibile.
Il mio più sentito ringraziamento va al professor Stefano Cacchione, che con la sua presenza (e soprattutto con la sua infinita pazienza) mi ha dato modo di maturare scientificamente, di approfondire ed ampliare le mie conoscenze, offrendomi la possibilità di confronto costante per ogni dubbio, perplessità o semplice riflessione e mettendo sempre a disposizione la sua ineccepibile competenza ed esperienza in campo molecolare, sia per lo svolgimento tecnico del lavoro che per l'intera stesura della tesi. Senza il suo contributo fondamentale, non avrei avuto la possibilità di lavorare ad un progetto così innovativo e rilevante, seppur insidioso e di complesso avanzamento.
Un ringraziamento particolare va anche alle sue due storiche collaboratrici, la dott.ssa Alessandra Galati e la dott.ssa Emanuela Micheli, per la loro disponibilità, il loro supporto professionale e morale. Seppur in modi diversi, entrambe hanno avuto la capacità di rendere fin dal principio il laboratorio un luogo adatto all'apprendimento e al confronto, gestendolo con rigore ma con grande umanità, sostenendomi in tutte le fasi importanti del percorso.
Non posso fare a meno di ringraziare il Dr. Armando Olivieri, il quale è riuscito a dare un contributo di grande rilevanza al progetto e con il quale ho condiviso una parte importante del mio dottorato, a cui ripenso con tanto affetto, stima e simpatia.
Ringrazio il professor Gian Gaetano Tartaglia e il Dr Alessio Colantoni per la professionalità, la competenza e la propositività con cui si sono occupati delle analisi bioinformatiche riguardanti il Nanopore sequencing. Nonostante sia un campo assolutamente

innovativo, sono riusciti ad ottenere risultati di grande qualità e rilevanza, necessari per l'avanzamento del progetto di ricerca.
Ringrazio inoltre la correlatrice della tesi, la dott.ssa Annamaria Biroccio, che mi ha dato la possibilità di intraprendere questo percorso formativo. Anche se la conduzione di un progetto in collaborazione non è stata semplice, mi ha permesso di imparare a gestire le dinamiche del mondo della ricerca e in generale del mondo del lavoro. La ringrazio inoltre di avermi dato la possibilità di continuare a lavorare nel suo gruppo di ricerca, che si è riconfermato, dopo ormai cinque anni di collaborazione, ricco di persone scientificamente valide e professionalmente qualificate, che mi hanno insegnato tanto (non solo durante il periodo di dottorato) e che non si sono mai sottratte ad una richiesta di aiuto o di confronto di natura scientifica e non. Il mio traguardo lo devo sicuramente anche a loro, a cui mi sento legata indissolubilmente da tanta stima e profondo affetto.
Tra tutti, mi sento in dovere di ringraziare in particolar modo la dott.ssa Angela Rizzo, la quale mi ha guidata durante il percorso di dottorato. Nonostante tutte le difficoltà incontrate, è sempre stata pronta a darmi una mano concreta, sia a livello sperimentale che analitico e interpretativo dei dati. La sua competenza in campo telomerico l'hanno resa un punto di riferimento assolutamente prezioso per l'avanzamento del progetto e per lo scioglimento dei punti critici incontrati durante il lavoro. Credo sia molto facile farsi invadere dall'entusiasmo all'inizio di un percorso, ma una ricerca di qualità è fatta principalmente da rigore sperimentale, tanto studio e costanza, e lei molto più che con le parole, è stata per me un esempio concreto di tutto questo.
Ringrazio inoltre la dott.ssa Erica Salvati; anche se la nostra collaborazione è stata limitata durante questo lavoro, il suo sostegno relativo ad alcune scelte professionali è stato determinante per farmi acquisire consapevolezza delle mie possibilità, dissipando con schiettezza ma anche con disarmante semplicità molti timori e insicurezze.

Un sentito ringraziamento va alla mia famiglia che, come sempre e nonostante le difficoltà, ha rispettato e assecondato tutte le scelte fatte durante il percorso, facendomi sentire il loro appoggio anche a distanza.
Il dottorato è qualcosa a cui ci si dedica con dedizione ed impegno, ma che ti mette di fronte ai tuoi limiti, a tanti imprevisti e incidenti di percorso che a tratti rischiano di logorare o di frustrare lo spirito e la motivazione. Dunque, un gigantesco grazie va ai miei amici, a quelli vecchi e a quelli nuovi, per il sostegno costante (spesso purtroppo a distanza), l'affetto infinito e la pazienza incrollabile dimostrate in questi anni e spero, in quelli a venire. Se siete riusciti a sopportarmi durante il dottorato di ricerca, il nostro legame è davvero indissolubile.